RSC Advances

PAPER

View Article Online
View Journal | View Issue

Cite this: *RSC Adv.*, 2022, **12**, 16454

Ni^{II} NPs entrapped within a matrix of L-glutamic acid cross-linked chitosan supported on magnetic carboxylic acid-functionalized multi-walled carbon nanotube: a new and efficient multi-task catalytic system for the green one-pot synthesis of diverse heterocyclic frameworks†

Morteza Hasanpour Galehban, Behzad Zeynizadeh and Hossein Mousavi *

In the present study, a new L-glutamic acid cross-linked chitosan supported on magnetic carboxylic acid-functionalized multi-walled carbon nanotube (Fe_3O_4/*f*-MWCNT-CS-Glu) nanocomposite was prepared through a convenient one-pot multi-component sequential strategy. Then, nickel^{II} nanoparticles (Ni^{II} NPs) were entrapped within a matrix of the mentioned nanocomposite. Afterward, the structure of the as-prepared Fe_3O_4/*f*-MWCNT-CS-Glu/Ni^{II} nanosystem was elucidated by various techniques, including FT-IR, PXRD, SEM, TEM, SEM-based EDX and elemental mapping, ICP-OES, TGA/DTA, and VSM. In the next part of this research, the catalytic applications of the mentioned nickel^{II}-containing magnetic nanocomposite were assessed upon green one-pot synthesis of diverse heterocyclic frameworks, including bis-coumarins (**3a–n**), 2-aryl(or heteroaryl)-2,3-dihydroquinazolin-4(1*H*)-ones (**5a–r**), 9-aryl-3,3,6,6-tetramethyl-3,4,5,6,7,9-hexahydro-1*H*-xanthene-1,8(2*H*)-diones (**7a–n**), and 2-amino-4-aryl-7,7-dimethyl-5-oxo-5,6,7,8-tetrahydro-4*H*-chromene-3-carbonitriles (**9a–n**). The good-to-excellent yields of the desired products, satisfactory reaction rates, use of water solvent or solvent-free reaction medium, acceptable turnover numbers (TONs) and turnover frequencies (TOFs), along with comfortable recoverability and satisfying reusability of the as-prepared nanocatalyst for at least eight successive runs, and also easy work-up and purification procedures are some of the advantages of the current synthetic protocols.

Received 18th November 2021
Accepted 20th April 2022

DOI: 10.1039/d1ra08454b

rsc.li/rsc-advances

1. Introduction

The preparation of new catalytic systems has particular importance and a specific position in organic synthesis and green chemistry. In this regard, the use of non-hazardous, available, cost-effective, stable, and active platforms is receiving more attention. Chitosan (CS) as the only polycationic biopolymer, which is mostly obtained from the alkaline deacetylation of chitin, has been used in various areas, especially biomedicine,[1] drug delivery,[2] gene delivery,[3] vaccine delivery,[4] dentistry,[5] tissue engineering,[6] wound-healing dressing,[7] water remediation,[8] agriculture,[9] food packaging,[10] catalysis,[11] and many others. The existence of numerous alcoholic, primary amine, acetamide, and ether functional groups in the chitosan structure causes this biocompatible complex hetero-biopolymer to be given special attention as an exclusive organic system in catalysis development. Due to having the mentioned functional groups, chitosan has been able to participate in advanced non-magnetic and magnetic catalytic structures such as metal–organic frameworks (MOFs),[12] covalent organic frameworks (COFs),[13] graphene oxide (GO)- and/or ionic liquid (IL)-containing systems,[14,15] Schiff base-type platforms,[16] micro-reactors,[17] and so on. In recent years, the publication of numerous reports on the diverse and eye-catching applications of functionalized carbon nanotubes (CNTs), including single-walled carbon nanotubes (SWCNTs), double-walled carbon nanotubes (DWCNTs), and multi-walled carbon nanotubes (MWCNTs), especially in the field of catalysis, is a valid proof of the value of these carbon scaffolds.[18] Interaction between polysaccharides (particularly chitosan) and CNTs can pave the way for the development of new catalytic platforms, especially creating a gigantic CNT-CS-containing matrix with a high ability to immobilize diverse metal nanoparticles, heteropoly acids (HPAs), *etc.* Also, the CNTs are capable of increasing some of the chitosan attributes, such as mechanical properties.[19] On the

Department of Organic Chemistry, Faculty of Chemistry, Urmia University, Urmia, Iran. E-mail: 1hossein.mousavi@gmail.com

† Electronic supplementary information (ESI) available. See https://doi.org/10.1039/d1ra08454b

other hand, one of the significant properties of a suitable catalyst from the green chemistry point of view is the capability of easy and complete separation from the reaction environment. For this purpose, the magnetic-type catalysts are an interesting choice because they can be separated from the reaction pot with an external magnetic field that allows avoiding time-consuming separation procedures.[20]

Heterocyclic frameworks are among the most significant molecules for everyday life.[11a,21] They exist in the structure of various compounds such as drugs, natural products, bioactive substances, vitamins, veterinary products, and many others. Among the available synthetic methods for the heterocyclic scaffolds construction, one-pot multi-component reactions (MCRs) have been considered as a powerful and fantastic strategy owing to their short reaction times, simplicity, high selectivity, *etc.*[22] Notably, the one-pot MCRs have been classified in the first branch of green chemistry principles, *viz.* prevent waste. It is worthy to note that the twelve principles of green chemistry have gained significant attention, both from academia and industries, and give us a guideline for designing safer and eco-friendly methods in chemical synthesis.[23] In addition to catalysis and synthetic method, the environmentally benign reaction medium is another essential parameter in the green chemistry discipline. For this purpose, water is the most desirable choice because this medium is safe, environmentally friendly, readily available, and inexpensive compared to other organic solvents.[24] On the other hand, solventless medium (well-known as solvent-free reaction conditions) is a great technique to perform reactions without using any solvents. The solvent-free method has many advantages rather than solution conditions, including high yields, short reaction times, simple reaction procedures and milder conditions, easy work-up and purification, high selectivity, minimization of by-products, and so on.[25]

In continuation of our ongoing research program in organic synthesis and catalyst design,[26] we report herein a convenient two-step preparation method for the construction of a new gigantic multi-functional catalytic system through the entrapping of the nickel^{II} nanoparticles into a matrix of L-glutamic acid cross-linked chitosan supported on magnetic carboxylic acid-functionalized multi-walled carbon nanotube (Fe_3O_4/*f*-MWCNT-CS-Glu/Ni^{II}). Also, after the well characterization, the catalytic applications of the as-prepared Fe_3O_4/*f*-MWCNT-CS-Glu/Ni^{II} hybrid system investigated on the environmentally benign one-pot synthesis of various heterocyclic frameworks, including bis-coumarins (**3a–n**), 2-aryl(or heteroaryl)-2,3-dihydroquinazolin-4(1*H*)-ones (**5a–r**), 9-aryl-3,3,6,6-tetramethyl-3,4,5,6,7,9-hexahydro-1*H*-xanthene-1,8(2*H*)-diones (**7a–n**), and 2-amino-4-aryl-7,7-dimethyl-5-oxo-5,6,7,8-tetrahydro-4*H*-chromene-3-carbonitriles (**9a–n**) (Fig. 1). Notably, the literature scrutiny clearly shows the preparation of such magnetically gigantic nanohybrid systems is not only precious in catalysis science and organic synthesis but also could be attractive and beneficial in biomedicine, drug delivery, agriculture, wastewater treatment, various type of sensors, capturing carbon dioxide, and many others.

2. Results and discussion

2.1. Preparation and characterization of the Fe_3O_4/*f*-MWCNT-CS-Glu/Ni^{II} nanocomposite

In recent years, one-pot multi-component reactions are recognized as a reliable and green synthetic strategy in the preparation of gigantic frameworks and have a great place in material science. Based on this issue, we designed a new one-pot five-component sequential protocol for the L-glutamic acid cross-linked chitosan supported on magnetic carboxylic acid-functionalized multi-walled carbon nanotube (Fe_3O_4/*f*-MWCNT-CS-Glu) construction as an active, suitable, and gigantic platform for the trapping metal nanoparticles (Scheme 1). In the second step, we immobilized the nickel^{II} nanoparticles into a matrix of the prepared Fe_3O_4/*f*-MWCNT-CS-Glu nanocomposite. After the successful preparation of the Fe_3O_4/*f*-MWCNT-CS-Glu/Ni^{II} hybrid system, we characterized the structure of the as-prepared nickel^{II}-containing nanocomposite by Fourier transform infrared spectroscopy (FT-IR), powder X-ray diffraction (PXRD), scanning electron microscopy (SEM), transmission electron microscopy (TEM), SEM-based energy-dispersive X-ray (EDX) and elemental mapping, inductively coupled plasma-optical emission spectrometry (ICP-OES), thermogravimetric analysis/differential thermal analysis (TGA/DTA), and vibrating sample magnetometer (VSM) analysis.

The FT-IR spectroscopy of the Fe_3O_4, Fe_3O_4/*f*-MWCNT, Fe_3O_4/*f*-MWCNT-CS, Fe_3O_4/*f*-MWCNT-CS-Glu, and Fe_3O_4/*f*-MWCNT-CS-Glu/Ni^{II} systems was carried out using the potassium bromide (KBr) disk method, and all of the spectra were recorded in the region 400–4000 cm^{-1}. In the FT-IR spectrum of the bare Fe_3O_4 nanoparticles (NPs), the absorption band at 567 cm^{-1} is attributed to the vibrations of the Fe–O bonds, and also the characteristic bands that appeared at 1623 cm^{-1} and 3418 cm^{-1} are approved to the bending and stretching vibrations of the surface hydroxyl (–OH) groups and adsorbed water molecules, respectively (Fig. 2, curve a). Although in the FT-IR spectrum of the Fe_3O_4/*f*-MWCNT system (Fig. 2, curve b), some index peaks are related to MWCNT-CO_2H overlapped with Fe_3O_4 NPs (especially stretching vibrations of the hydroxyl group of –CO_2H), the two distinct (weak) peaks at 2922 cm^{-1} and 2859 cm^{-1} that belong to the –CH stretching mode of the *f*-MWCNT nanosystem are revealed. After adding chitosan (CS) to the Fe_3O_4/*f*-MWCNT structure, a series of amide bonds were created. In the FT-IR spectrum of the Fe_3O_4/*f*-MWCNT-CS scaffold (Fig. 2, curve c), the broad band peak at 3434 cm^{-1} is related to the stretching vibrations of the existed –NH_2, –NH–, and –OH functional groups. The peaks around 3000–2867 cm^{-1} belong to the C–H stretching vibrations of the –CH= (which belongs to the *f*-MWCNT structure) and –CH_2– (which belongs to the chitosan biopolymer structure) groups. Moreover, the C=O stretching vibrations and the –NH– bending vibrations of the created amide bonds were revealed at 1634 cm^{-1} and 1568 cm^{-1}, respectively. Also, the peak at 1455 cm^{-1} could belong to the stretching vibrations of the C–N or the C–O stretching of the secondary alcoholic groups and even the –CH_2– bending vibrations in chitosan. Moreover, the C–O stretching vibrations of the primary alcoholic groups in chitosan appeared at 1411 cm^{-1}. The

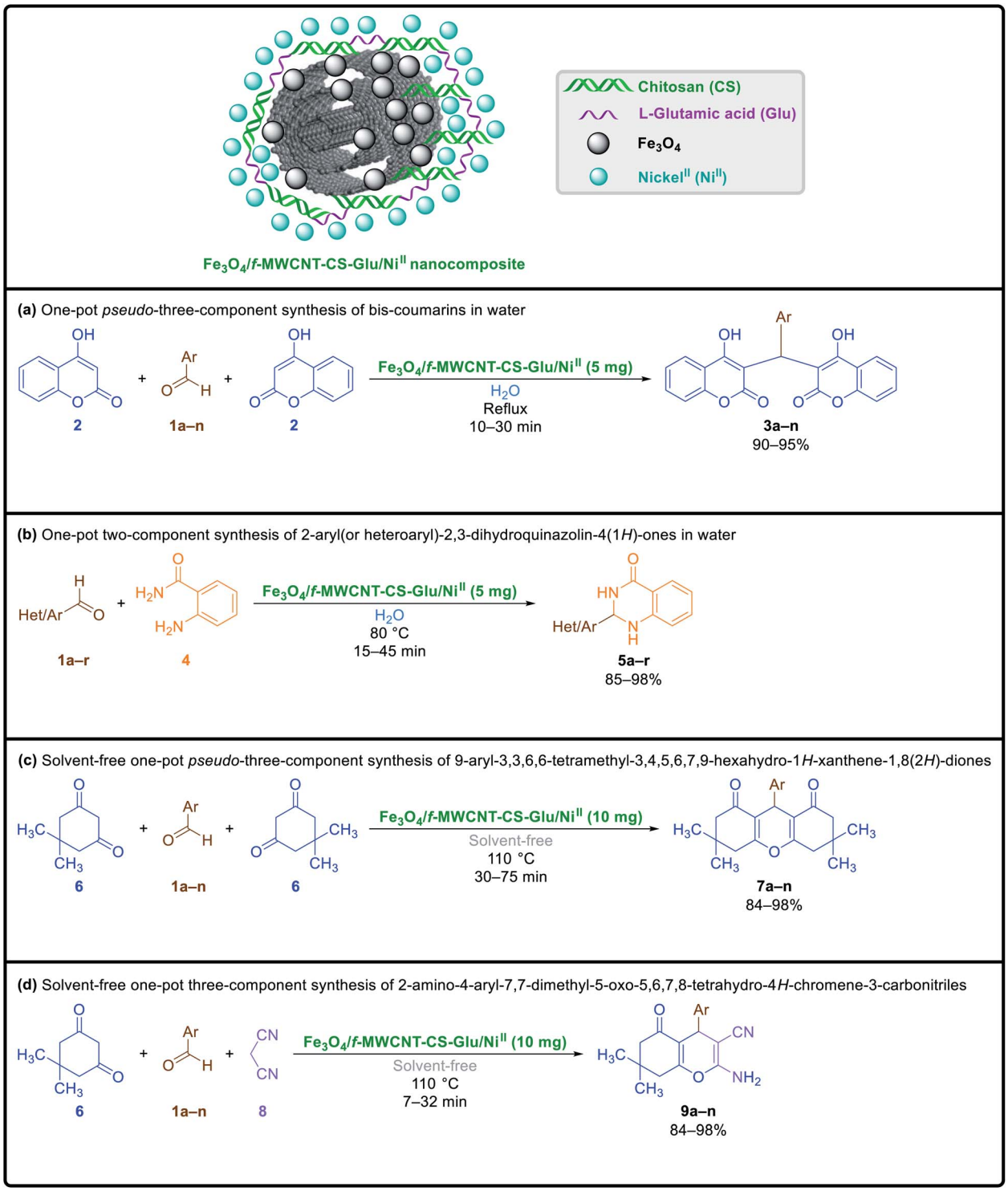

Fig. 1 Catalytic applications of the as-prepared Fe_3O_4/*f*-MWCNT-CS-Glu/Ni^{II} nanocomposite in the green one-pot multi-component synthesis of diverse heterocyclic frameworks.

bands at 1069 cm^{-1} and 1028 cm^{-1} display the C–O stretching vibrations of the etheric (C–O–C) and esteric bonds. Furthermore, the peaks at 800 cm^{-1}, 692 cm^{-1}, and 637 cm^{-1} related to the methylene and methine out-of-plane vibrations. Fig. 2 (curve d) showed the FT-IR spectrum of the Fe_3O_4/*f*-MWCNT-CS-Glu hybrid system, in which all the L-glutamic acid (Glu) functional groups peaks overlapped with some of the Fe_3O_4/*f*-MWCNT-CS peaks due to the similarity. Finally, in the FT-IR spectrum of the Fe_3O_4/*f*-MWCNT-CS-Glu/Ni^{II} magnetic nanocomposite (Fig. 2, curve e), all the distinct peaks (which thoroughly discussed above) were existed with a few differences due to the complexation of the –NH_2, –NH–, –OH, and C–O–C functional groups with the nickel^{II} nanoparticles.

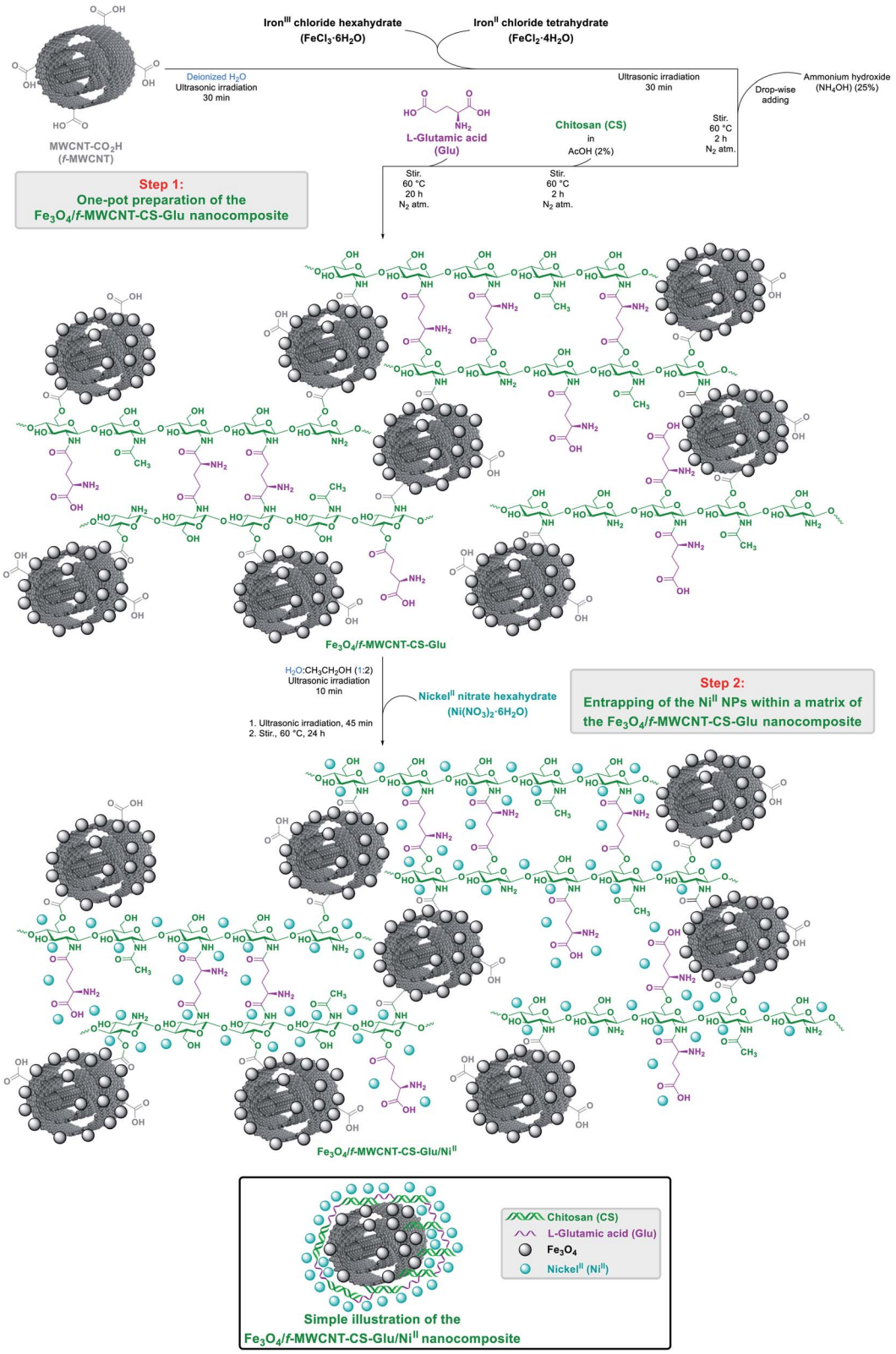

Scheme 1 Preparation of the Fe_3O_4/*f*-MWCNT-CS-Glu/Ni^{II} nanocomposite.

The powder X-ray diffraction (PXRD) spectra of the Fe_3O_4, Fe_3O_4/*f*-MWCNT, and Fe_3O_4/*f*-MWCNT-CS-Glu/Ni^{II} nanostructures are recorded in a range of Bragg's angle ($2\theta = 10–80°$) at room temperature (Fig. 3). In the PXRD pattern of the bare Fe_3O_4 NPs (Fig. 3, diagram a), nine diffraction peaks at (111), (220), (311), (400), (422), (511), (440), (620), and (553), which are

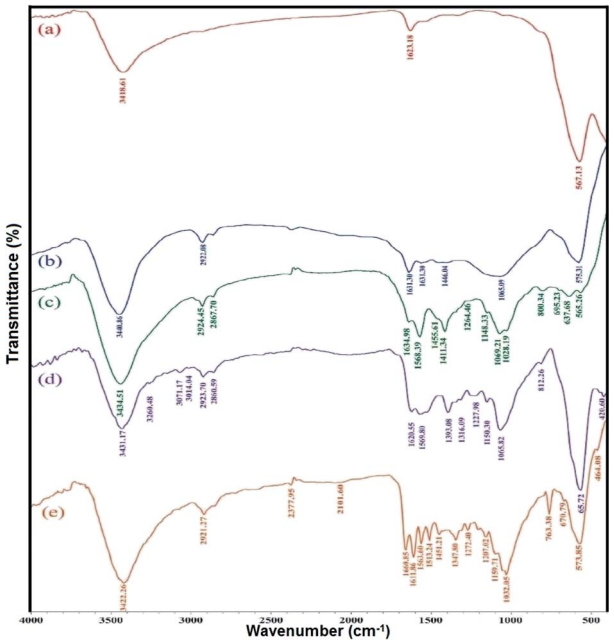

Fig. 2 FT-IR spectra of the (a) Fe_3O_4, (b) Fe_3O_4/*f*-MWCNT, (c) Fe_3O_4/*f*-MWCNT-CS, (d) Fe_3O_4/*f*-MWCNT-CS-Glu, and (e) Fe_3O_4/*f*-MWCNT-CS-Glu/Ni^{II} nanosystems.

indexed to the cubic spinel phase of Fe_3O_4, clearly appeared and matched well with Joint Committee on Powder Diffraction Standards (JCPDS) cards, file no. 79-0418, 65-3107, 74-2402, 01-075-0449, and 98-007-7842. In the Fe_3O_4/*f*-MWCNT PXRD pattern (Fig. 3, diagram b), in addition to the distinct peaks of the Fe_3O_4 NPs, a peak around $2\theta = 26°$ is related to the *f*-MWCNT structure. As shown in Fig. 3 (diagram c), the intensity of the $2\theta = 26°$ in the PXRD pattern of the Fe_3O_4/*f*-MWCNT-CS-Glu/Ni^{II} nanocomposite is increased, which could be related to the overlapping L-glutamic acid cross-linked chitosan (CS-Glu) peak with the *f*-MWCNT peak. Notably, the distinct peaks of the nickel^{II} NPs in the as-prepared nanocomposite structure were overlapped with some of the Fe_3O_4 NPs peaks.

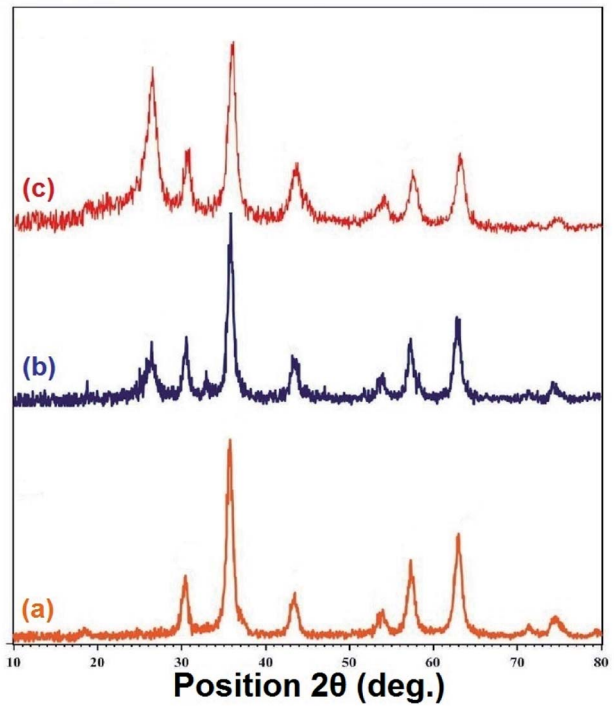

Fig. 3 PXRD patterns of the (a) Fe_3O_4, (b) Fe_3O_4/*f*-MWCNT, and (c) Fe_3O_4/*f*-MWCNT-CS-Glu/Ni^{II} nanosystems.

The morphology and size of the Fe_3O_4/*f*-MWCNT-CS-Glu/Ni^{II} hybrid nanocomposite were investigated by scanning electron microscopy (SEM) and transmission electron microscopy (TEM). The SEM images of the mentioned magnetic nanosystem (Fig. 4) indicated a spaghetti-like structure with a diameter of less than 44 nm related to the *f*-MWCNT and L-glutamic acid cross-linked chitosan (CS-Glu), which are surrounded by the Fe_3O_4 and nickel^{II} NPs. Also, in the Fe_3O_4/*f*-MWCNT-CS-Glu/Ni^{II} TEM images (Fig. 5), the existence of the Fe_3O_4 NPs and the entrapped Ni^{II} NPs into the matrix of the Fe_3O_4/*f*-MWCNT-CS-Glu nanocomposite can be seen clearly.

In order to further validate the composition elements of the as-prepared Fe_3O_4/*f*-MWCNT-CS-Glu/Ni^{II} nanocomposite, the SEM-based energy-dispersive X-ray (EDX) (Fig. 6) and elemental mapping (Fig. 7) analyses were performed. Both EDX and elemental mapping investigations confirm the presence of the carbon (C), nitrogen (N), oxygen (O), ferrite (Fe), and nickel (Ni) elements in the structure of the as-prepared gigantic hybrid nanosystem. The presence of the nickel element in the EDX and elemental mapping analyses inferred that the nickel^{II} NPs were successfully entrapped into the matrix of the Fe_3O_4/*f*-MWCNT-CS-Glu nanocomposite. Also, the EDX analysis gives the percentage of the elements, including 29.10 w%, 0.32 w%, 2.28 w%, 46.27 w%, and 22.03 w% for C, N, O, Fe, and Ni, respectively. Notably, the exact amount of the entrapped nickel is 12.32 w% based on the inductively coupled plasma-optical emission spectrometry (ICP-OES) measurement.

Thermogravimetric analysis/differential thermal analysis (TGA/DTA) was carried out to assess the thermal stability of the as-prepared Fe_3O_4/*f*-MWCNT-CS-Glu/Ni^{II} nanocomposite by heating it up to 800 °C under a nitrogen gas atmosphere (Fig. 8). In the first step, a weight loss (1%) occurred below 240 °C is related to the solvents and moisture evaporations. In the second step, a weight loss (9%) is observed at temperature ranging from 240 °C to 352 °C, which is mainly associated to the decomposition of L-glutamic acid[27] (as the cross-linker) and also is corresponding to the dehydration and depolymerization of the chitosan biopolymer.[28] In the third stage, a weight loss (6%) is observed between temperature range of 352 °C to 542 °C attributed to the complete decomposition of the chitosan structure by degasification of compounds, including NH_3, CO, CO_2, and CH_4.[29] In the final step, a weight loss (12%) is observed between temperature range of 542 °C to approximately 800 °C could be related to the pyrolysis and destruction of the *f*-MWCNT network.[30] It is worthwhile to note that the results of the TGA/DTA diagram confirm that the as-prepared Fe_3O_4/*f*-MWCNT-CS-Glu/Ni^{II} nanocomposite has

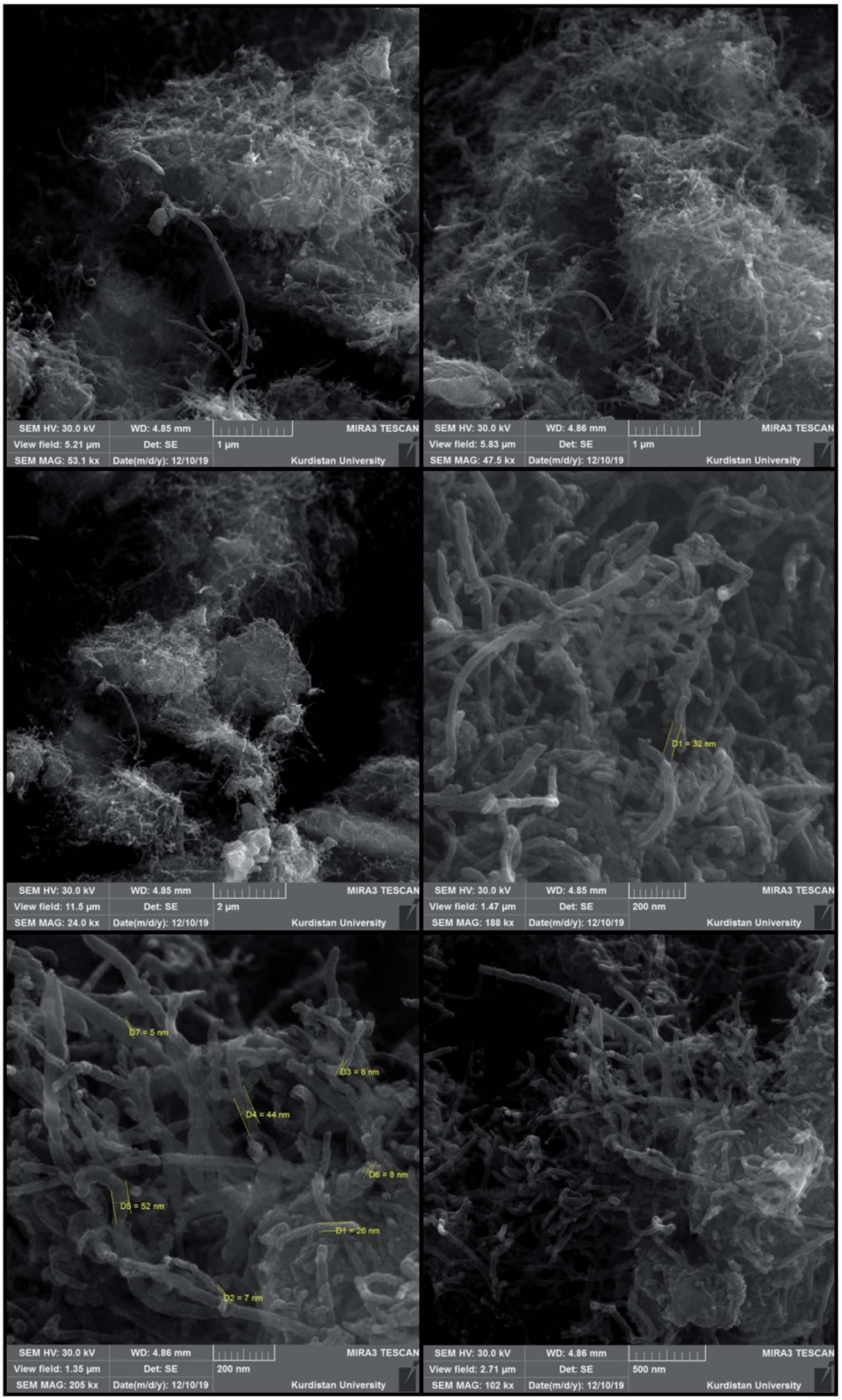

Fig. 4 SEM images of the as-prepared Fe_3O_4/*f*-MWCNT-CS-Glu/Ni^{II} nanocomposite.

enough and satisfactory stability to endure harsh temperature conditions up to 240 °C, which is so suitable for a catalytic system in organic synthesis.

The magnetic behavior of the prepared Fe_3O_4, Fe_3O_4/*f*-MWCNT, and Fe_3O_4/*f*-MWCNT-CS-Glu/Ni^{II} nanostructures was investigated by a vibrating sample magnetometer (VSM)

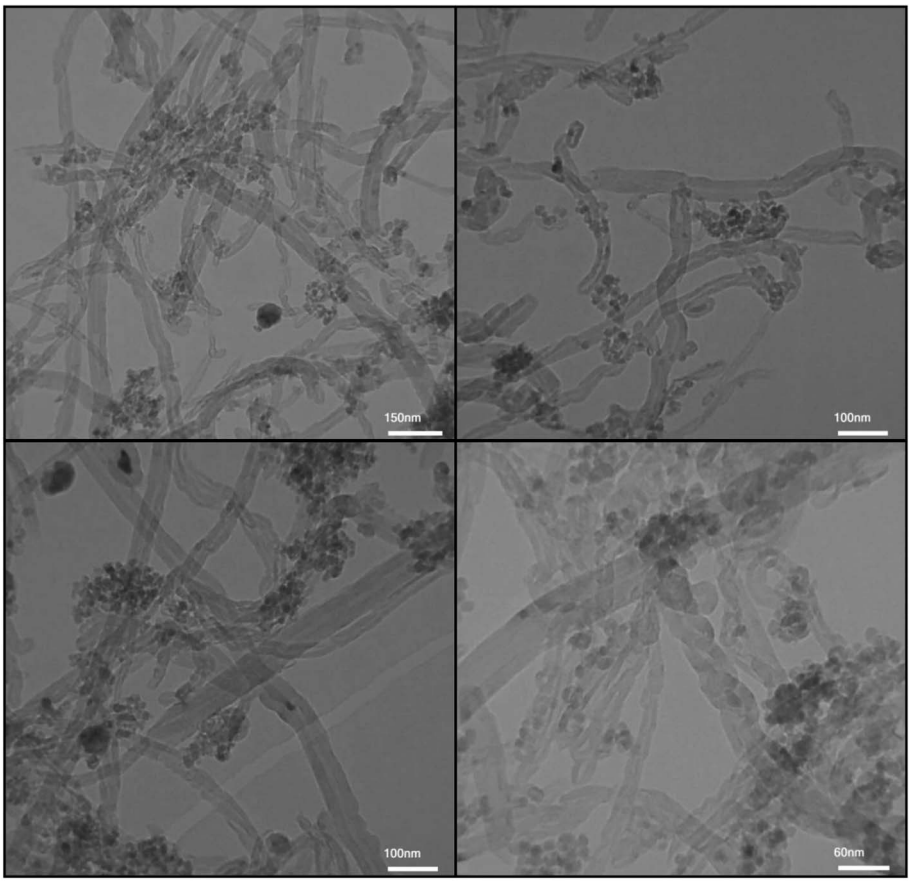

Fig. 5 TEM images of the as-prepared Fe_3O_4/*f*-MWCNT-CS-Glu/Ni^{II} nanocomposite.

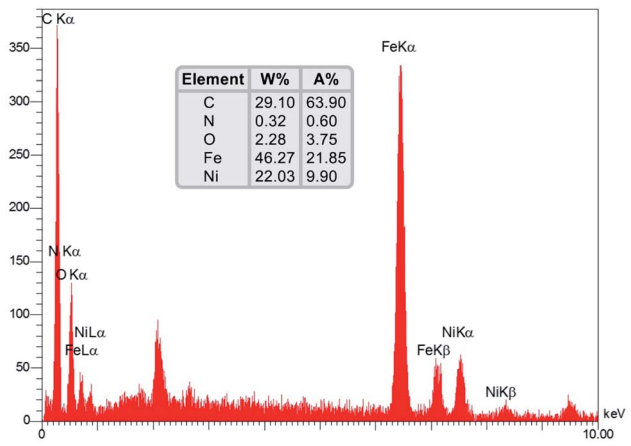

Fig. 6 SEM-based EDX diagram of the as-prepared Fe_3O_4/*f*-MWCNT-CS-Glu/Ni^{II} nanocomposite.

analysis at room temperature (Fig. 9). As it could be perceived from the resulting magnetization curves, the saturation magnetization (M_s) amounts of the Fe_3O_4, Fe_3O_4/*f*-MWCNT, and Fe_3O_4/*f*-MWCNT-CS-Glu/Ni^{II} nanosystems were 66.496 emu g^{-1}, 46.519 emu g^{-1}, and 19.743 emu g^{-1}, respectively. The decrease in the M_s amount of the as-prepared Fe_3O_4/*f*-MWCNT-CS-Glu/Ni^{II} nanocomposite rather than Fe_3O_4/*f*-MWCNT and bare Fe_3O_4 is attributed to the successful attaching L-glutamic acid cross-linked chitosan (CS-Glu) on the surface of the Fe_3O_4/*f*-MWCNT magnetic system and immobilization of the nickel^{II} NPs into the matrix of the Fe_3O_4/*f*-MWCNT-CS-Glu nanocomposite.

2.2. Catalytic applications of the as-prepared Fe_3O_4/*f*-MWCNT-CS-Glu/Ni^{II} nanocomposite

2.2.1. One-pot *pseudo*-three-component synthesis of bis-coumarins. After preparation and characterization of the Fe_3O_4/*f*-MWCNT-CS-Glu/Ni^{II} nanocomposite, to the demonstration of application merits of this new hybrid nanostructured catalyst in organic synthesis, we applied it in the one-pot synthesis of some valuable heterocyclic frameworks. In the first step, the one-pot synthesis of bis-coumarins (**3a–n**) was investigated. In order to optimize the reaction conditions, the simple one-pot *pseudo*-three-component synthesis of 3,3′-(phenylmethylene)bis(4-hydroxy-2*H*-chromen-2-one) (**3a**) through a condensation reaction between benzaldehyde (**1a**) and 4-hydroxycoumarin (**2**) was chosen as a model reaction. In the first step, the mentioned one-pot reaction was carried out in the presence of the as-prepared catalyst (5 mg) in several solvents, including water (H_2O), methanol (CH_3OH), ethanol (CH_3CH_2OH), acetonitrile (CH_3CN), ethyl acetate (EtOAc), dichloromethane (CH_2Cl_2), and *n*-hexane, and also under

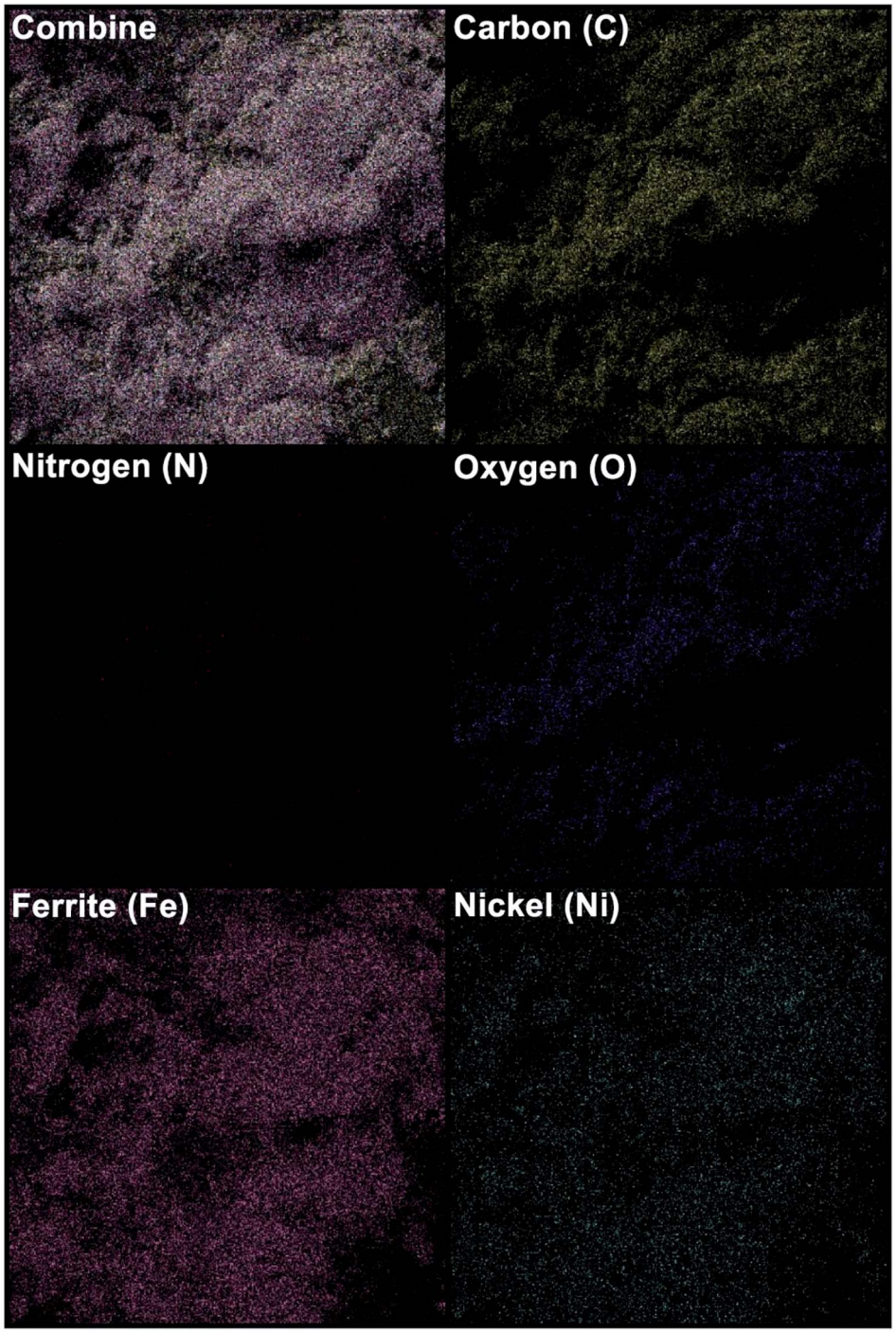

Fig. 7 SEM-based elemental mapping of the as-prepared Fe_3O_4/*f*-MWCNT-CS-Glu/Ni^{II} nanocomposite.

solvent-free conditions (Table 1). Although the obtained yield in water (Table 1, entry 1), ethanol (Table 1, entry 5), and solventless (Table 1, entry 10) mediums were high and the same (*viz.* 95%), the reaction rate in water and ethanol under reflux was faster than in solvent-free conditions at 70 °C. Based on obtained results and have respect to the green chemistry protocols, we selected water as the best and environmentally benign solvent for this one-pot reaction. Then, we examined the effect of less than (Table 1, entry 2) and more than (Table 1, entry 3) 5 mg of the as-prepared Fe_3O_4/*f*-MWCNT-CS-Glu/Ni^{II} catalyst on the synthesis of **3a** in water under reflux conditions and it was found that the optimal amount of the catalyst loading is 5 mg. Furthermore and to show the importance and effect of the as-prepared Ni^{II}-containing nanocatalyst on the synthesis of **3a**, we designed and carried out some control experiments using component parts of the Fe_3O_4/*f*-MWCNT-CS-Glu/Ni^{II} nanocomposite (Table 1, entries 11–14). To our delight, the control experiments results showed that the

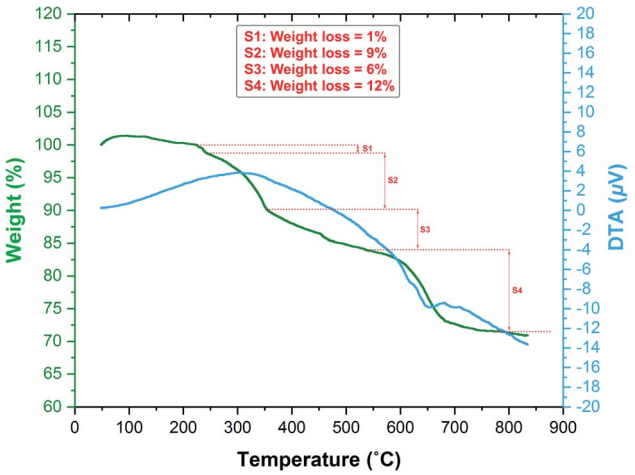

Fig. 8 TGA/DTA diagram of the as-prepared Fe_3O_4/*f*-MWCNT-CS-Glu/Ni^{II} nanocomposite.

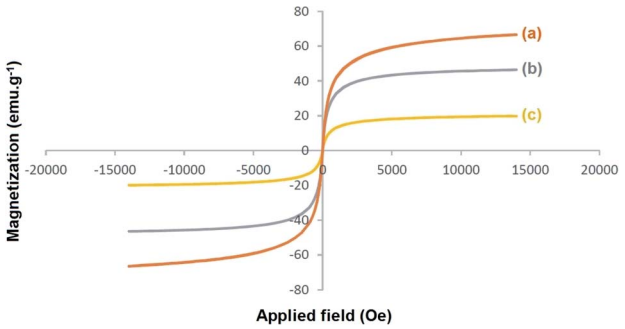

Fig. 9 Magnetization curves of the prepared (a) Fe_3O_4, (b) Fe_3O_4/*f*-MWCNT, and (c) Fe_3O_4/*f*-MWCNT-CS-Glu/Ni^{II} nanosystems.

catalytic effect of the mentioned nanocomposite is definitely better than its components. After optimizing the reaction conditions, we next examined the substrate scope for the mentioned one-pot *pseudo*-three-component reaction using diverse aromatic aldehyde derivatives (Scheme 2). Interestingly, both the electron-donating and electron-withdrawing groups (EDGs and EWGs) on aryl aldehydes were found tolerable to reaction conditions and provided products (**3a–n**) in good-to-excellent yields. Also, the turnover numbers (TONs) and turnover frequencies (TOFs) of the Fe_3O_4/*f*-MWCNT-CS-Glu/Ni^{II} nanocatalyst in this one-pot *pseudo*-three-component synthesis of bis-coumarins (**3a–n**) were calculated. As shown in Scheme 2, the determined TONs and TOFs are acceptable and satisfactory. The chemical structures of the synthesized bis-coumarins (**3a–n**) were characterized by FT-IR, ^{1}H NMR, and melting points, and compared with authentic literature. Furthermore, a plausible mechanism for this valuable tandem Knoevenagel–Michael condensation in the presence of the as-prepared Fe_3O_4/*f*-MWCNT-CS-Glu/Ni^{II} hybrid nanocatalytic system is depicted in Scheme 3. Briefly, in the first stage, aromatic aldehyde (**1a–n**) activated by the as-prepared Fe_3O_4/*f*-MWCNT-CS-Glu/Ni^{II} nanocomposite (especially by the Ni^{II} section) and then the nucleophilic attack of 4-hydroxycoumarin (**2**) to the mentioned activated aryl aldehyde caused the elimination of one water molecule and formation of the 3-benzylidenechromane-2,4-dione intermediate (**IA**). Next, the Michael addition of another 4-hydroxycoumarin (**2**) to the activated α,β-unsaturated carbonyl compound (**IA**) yielded corresponding bis-coumarins (**3a–n**).

2.2.2. One-pot two-component synthesis of 2-aryl(or heteroaryl)-2,3-dihydroquinazolin-4(1*H*)-ones. Another catalytic application of the as-prepared Fe_3O_4/*f*-MWCNT-CS-Glu/Ni^{II} nanocomposite investigated in the green and one-pot two-component synthesis of 2-aryl(or heteroaryl)-2,3-dihydroquinazolin-4(1*H*)-ones (**5a–r**). It is worthy to note that quinazolinones are fundamental building blocks in nature and part of the backbone of several naturally occurring alkaloids and biologically active compounds.[31] After optimization of the main reaction parameters (Table 2), which take place on the one-pot synthesis of 2-phenyl-2,3-dihydroquinazolin-4(1*H*)-one (**5a**) through a two-component reaction of benzaldehyde (**1a**) and 2-aminobenzamide (also known as anthranilamide) (**4**), the scope and limitation of the presented strategy studied using a wide range of aromatic and heteroaromatic aldehydes under the optimized reaction conditions (Table 2, entry 1). As shown in Scheme 4, all of the desired 2-aryl(or heteroaryl)-2,3-dihydroquinazolin-4(1*H*)-ones (**5a–r**) obtained in good-to-excellent yields in water at 80 °C in the presence of 5 mg of the mentioned Ni^{II}-containing nanocomposite. On the other hand, the TONs and TOFs of the Fe_3O_4/*f*-MWCNT-CS-Glu/Ni^{II} nanocatalyst in this one-pot two-component reaction have been measured and listed in Scheme 4. The chemical structures of the obtained 2-aryl(or heteroaryl)-2,3-dihydroquinazolin-4(1*H*)-ones (**5a–r**) were confirmed by FT-IR, ^{1}H NMR, and melting points, and compared with authentic papers. Also, a plausible mechanism for this green one-pot two-component reaction in the presence of the mentioned gigantic catalytic system is presented in Scheme 5. As shown in Scheme 5, in the first step, aromatic(or heteroaromatic) aldehyde (**1a–r**) was activated by the as-prepared catalytic system, and then the mentioned carbonyl group of aryl(or heteroaryl)aldehyde was attacked by the amine section of 2-aminobenzamide (**4**) that leads to the formation of the aldimine intermediate (**IB**) along with the elimination of one water molecule. In the next step, the activated **IB** intermediate converted to the **IIB** intermediate by the amide-iminol tautomerization process. After that, the **IIB** intermediate, which was activated by the Fe_3O_4/*f*-MWCNT-CS-Glu/Ni^{II} nanocomposite, generated desired product (**5a–r**) by an intramolecular heterocyclization pathway which occurs through a [1,5]-hydrogen transfer.

2.2.3. One-pot multi-component synthesis of fused 4*H*-pyrans. The results related to the impressive catalytic effect of the as-prepared Fe_3O_4/*f*-MWCNT-CS-Glu/Ni^{II} hybrid nanocomposite in the green one-pot synthesis of bis-coumarins (**3a–n**) and 2-aryl(or heteroaryl)-2,3-dihydroquinazolin-4(1*H*)-ones (**5a–r**) encouraged us to study and develop catalytic applications of this magnetic hybrid nanocatalyst in the environmentally benign one-pot multi-component synthesis of other heterocyclic frameworks as well. To this purpose, we selected 9-aryl-

Table 1 Optimization reaction conditions for the one-pot *pseudo*-three-component synthesis of **3a**

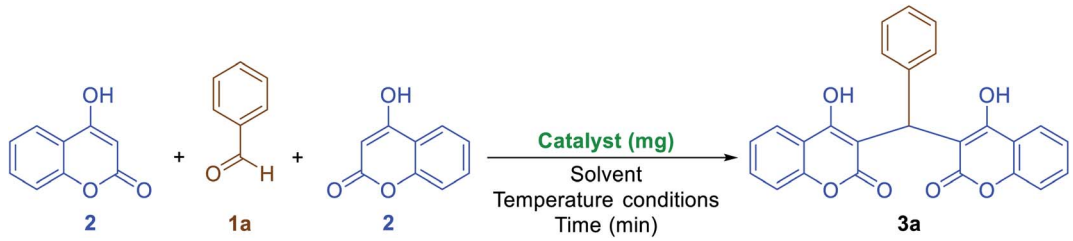

Entry	Catalyst	Catalyst loading (mg)	Solvent	Temperature conditions	Time (min)	Yield (%)
1	Fe_3O_4/*f*-MWCNT-CS-Glu/Ni^{II}	5	H_2O	Reflux	10	95
2	Fe_3O_4/*f*-MWCNT-CS-Glu/Ni^{II}	4	H_2O	Reflux	15	90
3	Fe_3O_4/*f*-MWCNT-CS-Glu/Ni^{II}	7	H_2O	Reflux	10	95
4	Fe_3O_4/*f*-MWCNT-CS-Glu/Ni^{II}	5	CH_3OH	Reflux	20	65
5	Fe_3O_4/*f*-MWCNT-CS-Glu/Ni^{II}	5	CH_3CH_2OH	Reflux	10	95
6	Fe_3O_4/*f*-MWCNT-CS-Glu/Ni^{II}	5	CH_3CN	Reflux	120	35
7	Fe_3O_4/*f*-MWCNT-CS-Glu/Ni^{II}	5	EtOAC	Reflux	120	25
8	Fe_3O_4/*f*-MWCNT-CS-Glu/Ni^{II}	5	CH_2Cl_2	35 °C	120	20
9	Fe_3O_4/*f*-MWCNT-CS-Glu/Ni^{II}	5	*n*-Hexane	Reflux	120	10
10	Fe_3O_4/*f*-MWCNT-CS-Glu/Ni^{II}	5	Solvent-free	70 °C	15	95
11	Fe_3O_4/*f*-MWCNT-CS-Glu	5	H_2O	Reflux	120	55
12	Fe_3O_4/*f*-MWCNT-CS	5	H_2O	Reflux	120	55
13	Fe_3O_4/*f*-MWCNT	5	H_2O	Reflux	120	50
14	Fe_3O_4	5	H_2O	Reflux	120	—

3,3,6,6-tetramethyl-3,4,5,6,7,9-hexahydro-1*H*-xanthene-1,8(2*H*)-diones (**7a–n**) and 2-amino-4-aryl-7,7-dimethyl-5-oxo-5,6,7,8-tetrahydro-4*H*-chromene-3-carbonitriles (**9a–n**) as two important heterocyclic systems of the fused 4*H*-pyrans family. The optimization studies upon model reactions (Tables 3 and 4) showed that both of the two mentioned heterocyclic compounds could be successfully synthesized under solvent-free conditions in the presence of 10 mg of the mentioned nanocatalyst at 110 °C. Further studies on the scope and generality of the presented one-pot multi-component reactions indicated that the desired 9-aryl-3,3,6,6-tetramethyl-3,4,5,6,7,9-hexahydro-1*H*-xanthene-1,8(2*H*)-diones (**7a–n**) (Scheme 6) and 2-amino-4-aryl-7,7-dimethyl-5-oxo-5,6,7,8-tetrahydro-4*H*-chromene-3-carbonitriles (**9a–n**) (Scheme 7) could be obtained in relatively good-to-excellent yields under the optimal reaction conditions. Furthermore, the TONs and TOFs of the as-prepared Fe_3O_4/*f*-MWCNT-CS-Glu/Ni^{II} hybrid nanocatalyst in these one-pot reactions have been measured and listed in Schemes 6 and 7. The chemical structures of the synthesized fused 4*H*-pyrans (**7a–n**) and (**9a–n**) were confirmed by FT-IR, ^{1}H NMR, and melting points, and compared with authentic papers. Also, the plausible mechanisms for these solvent-free one-pot multi-component reactions in the presence of the Fe_3O_4/*f*-MWCNT-CS-Glu/Ni^{II} gigantic catalytic system are presented in Schemes 8 and 9. As shown in Scheme 8, the formation of 9-aryl-3,3,6,6-tetramethyl-3,4,5,6,7,9-hexahydro-1*H*-xanthene-1,8(2*H*)-diones (**7a–n**) *via* the presented one-pot *pseudo*-three-component synthetic strategy started with the activation of the carbonyl group of aryl aldehyde (**1a–n**) by the Fe_3O_4/*f*-MWCNT-CS-Glu/Ni^{II} nanocatalyst and subsequently nucleophilic attack of dimedone (**6**) that leads to the formation of the Knoevenagel intermediate (**IC**) along with the elimination of one water molecule. In the next step, the Michael addition of the second dimedone molecule (**6**) upon activated **IC** caused the formation of **IIC**. In the final step, intramolecular cyclization of the activated **IIC** occurs after the successful elimination of another water molecule resulted desired xanthene (**7a–n**) and regenerated Fe_3O_4/*f*-MWCNT-CS-Glu/Ni^{II} magnetic nanocatalyst into the reaction pot. Also, as shown in Scheme 9, the reaction mechanism of the formation of 2-amino-4-aryl-7,7-dimethyl-5-oxo-5,6,7,8-tetrahydro-4*H*-chromene-3-carbonitriles (**9a–n**) in the presence of the as-prepared Ni^{II}-containing nanocatalyst started by the formation of the arylidienemalononitrile intermediate (**ID**) and releasing one water molecule *via* the Knoevenagel condensation between malononitrile (**8**) and the activated aromatic aldehyde (**1a–n**). Next, the Michael addition of the dimedone molecule (**6**) to the activated arylidienemalononitrile (**ID**) occurred to form **IID** intermediate. Finally, the intramolecular cyclization of the activated **IID** intermediate resulted desired fused heterocyclic product (**9a–n**).

2.3. Recoverability, reusability, leaching, and hot filtration test studies of the as-prepared Fe_3O_4/*f*-MWCNT-CS-Glu/Ni^{II} nanocomposite

Easy recovery and high reusability of catalyst are remarkably significant factors, exclusively for commercial and industrial applications and also from the green chemistry point of view. In this line, we performed some experiments to investigate the

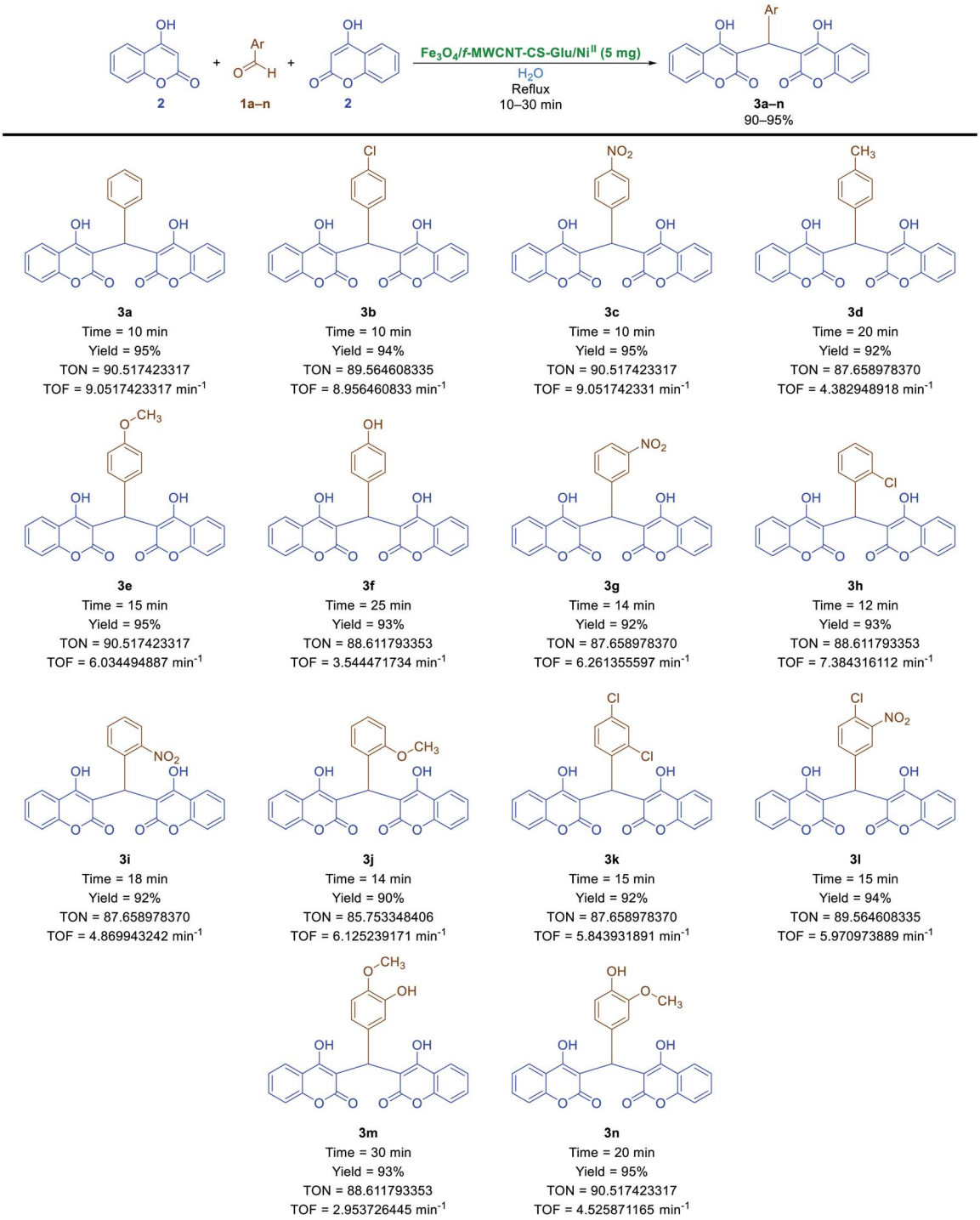

TON (Turnover number) = [(mol of product formed) / (mol of catalyst used)]
TOF (Turnover frequency) = [(mol of product formed) / (mol of catalyst used) × (time)]

Note:

The TONs and TOFs values were calculated based on the existed amount of nickel (Ni) in the as-prepared nanocatalyst (in 5 mg of the nanocatalyst, 0.616 mg (or 0.010495217 mmol) of Ni has existed).

Scheme 2 One-pot *pseudo*-three-component synthesis of bis-coumarins in water catalyzed by the as-prepared Fe_3O_4/*f*-MWCNT-CS-Glu/Ni^{II} nanocomposite.

catalyst recyclability for all the aforesaid four model organic reactions on the one-pot synthesis of **3a**, **5a**, **7a**, and **9a** under the optimized reaction conditions. To do this and after each investigation, the catalyst was separated from the reaction pot with a magnet. Next, the isolated nickel^{II}-containing catalyst was washed, dried, and then directly used in the next run of the

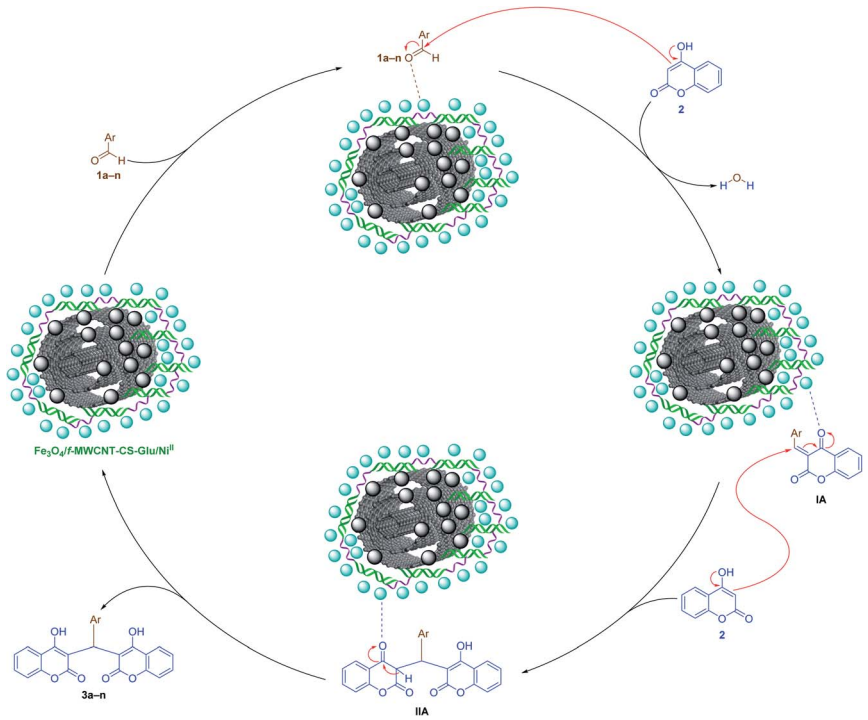

Scheme 3 Plausible mechanism for the one-pot *pseudo*-three-component synthesis of bis-coumarins in the presence of the as-prepared Fe_3O_4/*f*-MWCNT-CS-Glu/Ni^{II} nanocatalyst.

reaction. As shown in Fig. 10, the recoverability and reusability experiments of the Fe_3O_4/*f*-MWCNT-CS-Glu/Ni^{II} nanocomposite revealed satisfactory results even after eight runs for all the four mentioned one-pot synthetic protocols. On the other hand, in order to evaluation of the Fe_3O_4/*f*-MWCNT-CS-Glu/Ni^{II} stability into the reaction environment, we carried out leaching tests, which were investigated on the one-pot two-component synthesis of 2-phenyl-2,3-dihydroquinazolin-4(1*H*)-one (**5a**).

Table 2 Optimization reaction conditions for the one-pot two-component synthesis of **5a**

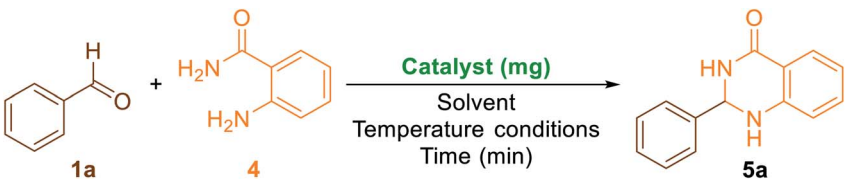

Entry	Catalyst	Catalyst loading (mg)	Solvent	Temperature conditions	Time (min)	Yield (%)
1	Fe_3O_4/*f*-MWCNT-CS-Glu/Ni^{II}	5	H_2O	80 °C	20	98
2	Fe_3O_4/*f*-MWCNT-CS-Glu/Ni^{II}	4	H_2O	80 °C	20	92
3	Fe_3O_4/*f*-MWCNT-CS-Glu/Ni^{II}	7	H_2O	80 °C	20	98
4	Fe_3O_4/*f*-MWCNT-CS-Glu/Ni^{II}	5	CH_3OH	Reflux	30	84
5	Fe_3O_4/*f*-MWCNT-CS-Glu/Ni^{II}	5	CH_3CH_2OH	Reflux	20	98
6	Fe_3O_4/*f*-MWCNT-CS-Glu/Ni^{II}	5	CH_3CN	Reflux	30	90
7	Fe_3O_4/*f*-MWCNT-CS-Glu/Ni^{II}	5	EtOAc	Reflux	90	50
8	Fe_3O_4/*f*-MWCNT-CS-Glu/Ni^{II}	5	CH_2Cl_2	35 °C	120	25
9	Fe_3O_4/*f*-MWCNT-CS-Glu/Ni^{II}	5	*n*-Hexane	Reflux	120	15
10	Fe_3O_4/*f*-MWCNT-CS-Glu/Ni^{II}	5	THF	Reflux	120	70
11	Fe_3O_4/*f*-MWCNT-CS-Glu/Ni^{II}	5	Solvent-free	70 °C	15	95
12	Fe_3O_4/*f*-MWCNT-CS-Glu	5	H_2O	80 °C	120	30
13	Fe_3O_4/*f*-MWCNT-CS	5	H_2O	80 °C	120	10
14	Fe_3O_4/*f*-MWCNT	5	H_2O	80 °C	120	10
15	Fe_3O_4	5	H_2O	80 °C	120	—

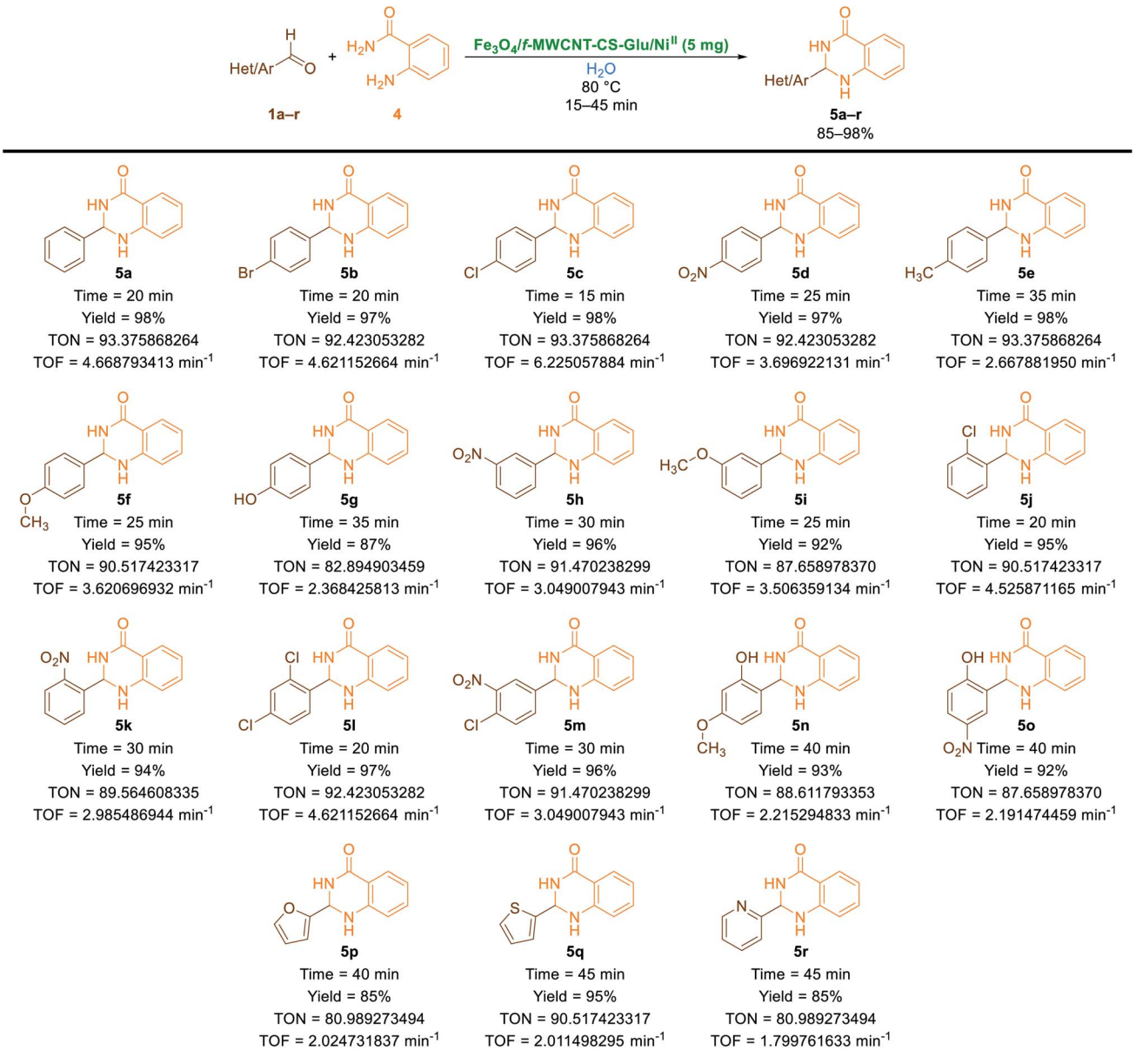

Scheme 4 One-pot two-component synthesis of 2-aryl(or heteroaryl)-2,3-dihydroquinazolin-4(1*H*)-ones catalyzed by the as-prepared Fe_3O_4/*f*-MWCNT-CS-Glu/Ni^{II} nanocomposite in water.

The leaching tests results obtained by ICP-OES measurements showed that the amount of nickel (Ni) after the fourth and eighth reaction cycles was 11.08 w% and 9.74 w%, respectively. The hot filtration test was also performed for the further investigation upon leaching of the Ni^{II} NPs on the one-pot synthesis of **5a** in the water solvent. As shown in Fig. 11, we separated the whole of the as-prepared Fe_3O_4/*f*-MWCNT-CS-Glu/Ni^{II} nano-based catalytic system from the mentioned reaction environment (when the conversion rate was 60%), and it was found that after filtration and in the absence of the aforesaid Ni^{II}-containing catalyst, almost no significant improvement was seen in the reaction process. The conversion rate of the reaction in this stage confirms the leaching of Ni^{II} was negligible. Furthermore, the PXRD diagram (Fig. 12) of the recycled Fe_3O_4/*f*-MWCNT-CS-Glu/Ni^{II} catalytic system after the third recycling step with those of the fresh one shows that the structure of the mentioned hybrid nanocomposite remained intact.

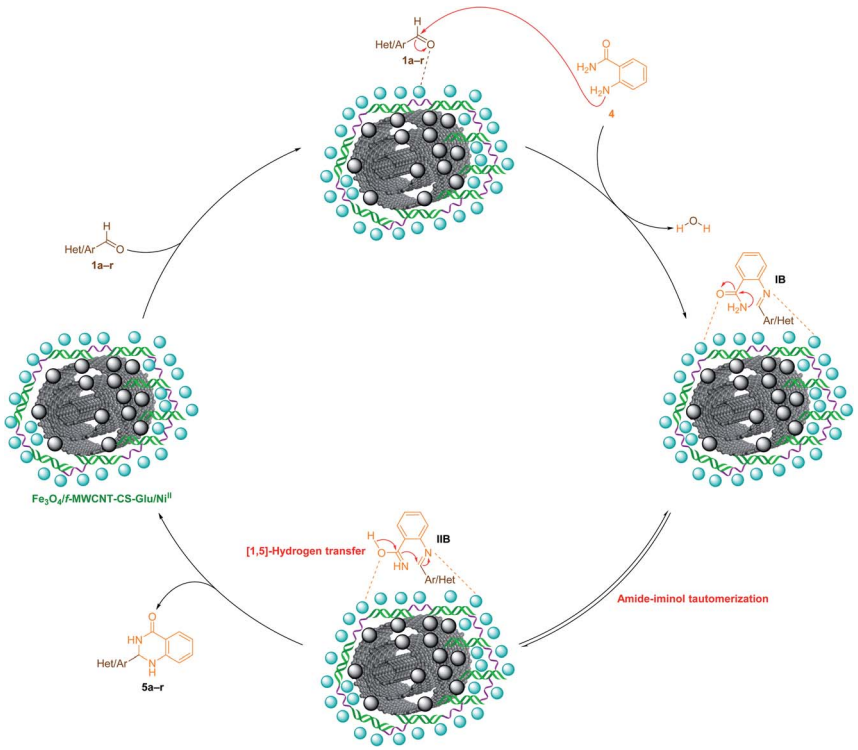

Scheme 5 Plausible mechanism for the one-pot two-component synthesis of 2-aryl(or heteroaryl)-2,3-dihydroquinazolin-4(1*H*)-ones catalyzed by the as-prepared Fe_3O_4/*f*-MWCNT-CS-Glu/Ni^{II} nanocomposite in water.

Table 3 Optimization reaction conditions for the one-pot *pseudo*-three-component synthesis of **7a**

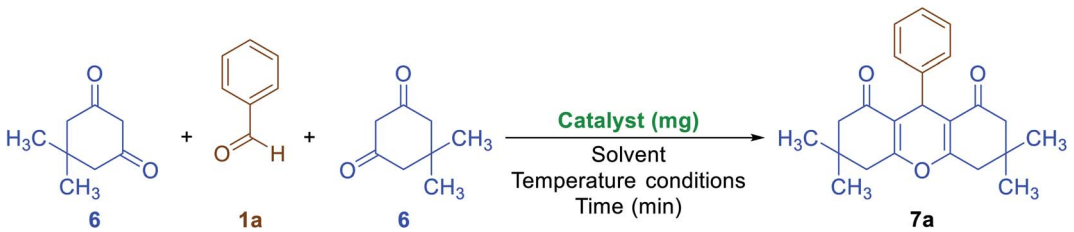

Entry	Catalyst	Catalyst loading (mg)	Solvent	Temperature conditions	Time (min)	Yield (%)
1	Fe_3O_4/*f*-MWCNT-CS-Glu/Ni^{II}	10	H_2O	Reflux	120	50
2	Fe_3O_4/*f*-MWCNT-CS-Glu/Ni^{II}	10	CH_3OH	Reflux	40	70
3	Fe_3O_4/*f*-MWCNT-CS-Glu/Ni^{II}	10	CH_3CH_2OH	Reflux	40	78
4	Fe_3O_4/*f*-MWCNT-CS-Glu/Ni^{II}	10	CH_3CN	Reflux	180	65
5	Fe_3O_4/*f*-MWCNT-CS-Glu/Ni^{II}	10	EtOAc	Reflux	180	25
6	Fe_3O_4/*f*-MWCNT-CS-Glu/Ni^{II}	10	CH_2Cl_2	35 °C	120	10
7	Fe_3O_4/*f*-MWCNT-CS-Glu/Ni^{II}	10	*n*-Hexane	Reflux	180	20
8	Fe_3O_4/*f*-MWCNT-CS-Glu/Ni^{II}	10	THF	Reflux	120	30
9	Fe_3O_4/*f*-MWCNT-CS-Glu/Ni^{II}	10	Solvent-free	110 °C	40	96
10	Fe_3O_4/*f*-MWCNT-CS-Glu/Ni^{II}	5	Solvent-free	110 °C	40	82
11	Fe_3O_4/*f*-MWCNT-CS-Glu/Ni^{II}	15	Solvent-free	110 °C	40	96
12	Fe_3O_4/*f*-MWCNT-CS-Glu	10	Solvent-free	110 °C	180	30
13	Fe_3O_4/*f*-MWCNT-CS	10	Solvent-free	110 °C	180	10
14	Fe_3O_4/*f*-MWCNT	10	Solvent-free	110 °C	180	10
15	Fe_3O_4	10	Solvent-free	110 °C	180	—

Table 4 Optimization reaction conditions for the one-pot three-component synthesis of **9a**

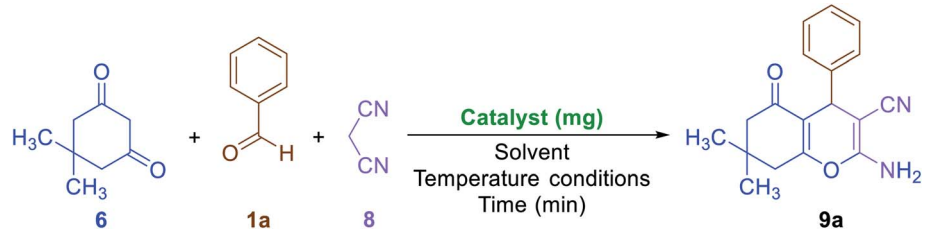

Entry	Catalyst	Catalyst loading (mg)	Solvent	Temperature conditions	Time (min)	Yield (%)
1	Fe_3O_4/*f*-MWCNT-CS-Glu/Ni^{II}	10	H_2O	Reflux	120	65
2	Fe_3O_4/*f*-MWCNT-CS-Glu/Ni^{II}	10	CH_3OH	Reflux	30	60
3	Fe_3O_4/*f*-MWCNT-CS-Glu/Ni^{II}	10	CH_3CH_2OH	Reflux	30	72
4	Fe_3O_4/*f*-MWCNT-CS-Glu/Ni^{II}	10	CH_3CN	Reflux	60	60
5	Fe_3O_4/*f*-MWCNT-CS-Glu/Ni^{II}	10	EtOAc	Reflux	80	15
6	Fe_3O_4/*f*-MWCNT-CS-Glu/Ni^{II}	10	CH_2Cl_2	35 °C	120	—
7	Fe_3O_4/*f*-MWCNT-CS-Glu/Ni^{II}	10	*n*-Hexane	Reflux	120	10
8	Fe_3O_4/*f*-MWCNT-CS-Glu/Ni^{II}	10	THF	Reflux	40	45
9	Fe_3O_4/*f*-MWCNT-CS-Glu/Ni^{II}	10	Solvent-free	110 °C	10	97
10	Fe_3O_4/*f*-MWCNT-CS-Glu/Ni^{II}	5	Solvent-free	110 °C	15	85
11	Fe_3O_4/*f*-MWCNT-CS-Glu/Ni^{II}	15	Solvent-free	110 °C	10	97
12	Fe_3O_4/*f*-MWCNT-CS-Glu	10	Solvent-free	110 °C	120	40
13	Fe_3O_4/*f*-MWCNT-CS	10	Solvent-free	110 °C	120	40
14	Fe_3O_4/*f*-MWCNT	10	Solvent-free	110 °C	120	30
15	Fe_3O_4	10	Solvent-free	110 °C	120	—

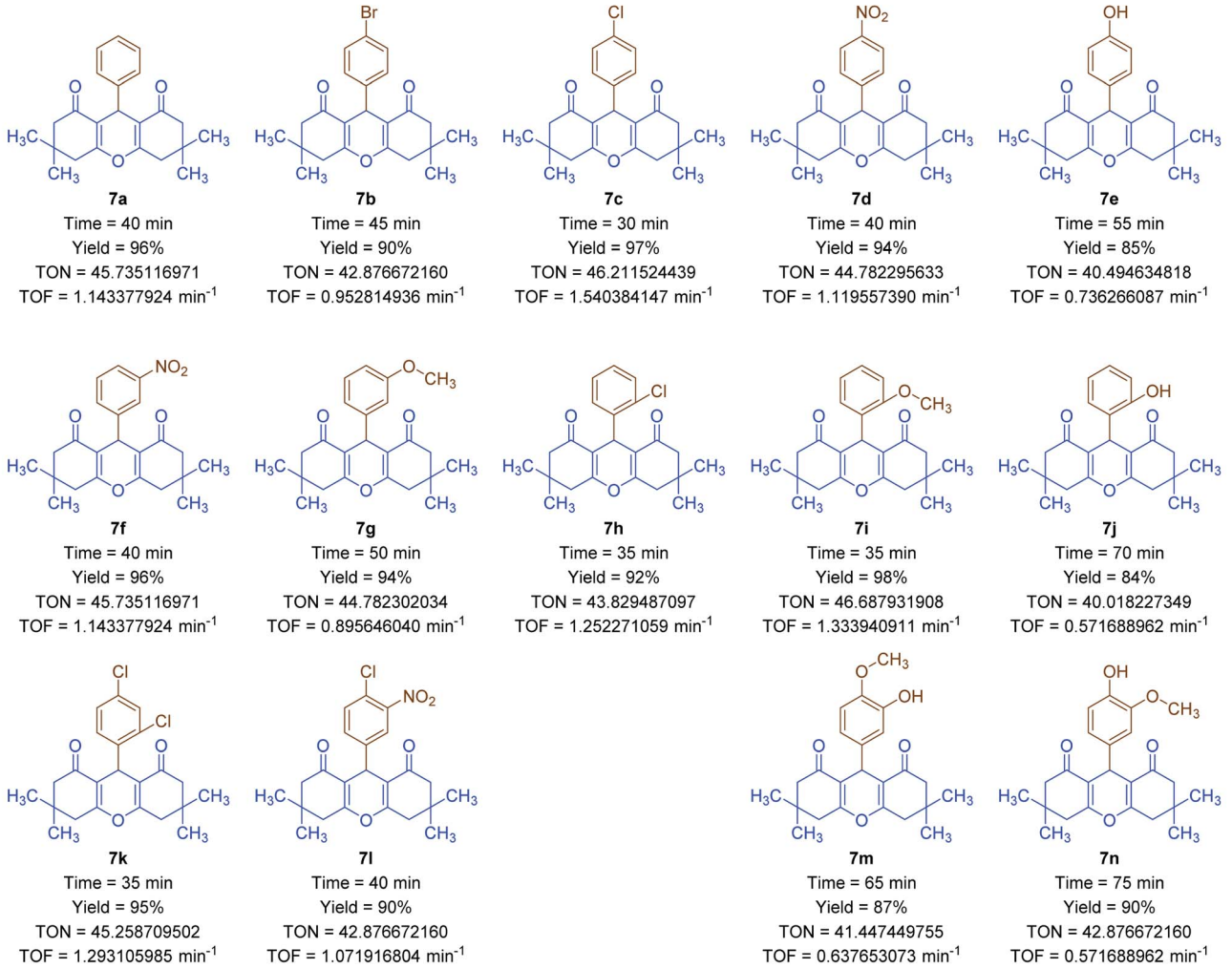

TON (Turnover number) = [(mol of product formed) / (mol of catalyst used)]
TOF (Turnover frequency) = [(mol of product formed) / (mol of catalyst used) × (time)]

Note:

The TONs and TOFs values were calculated based on the existed amount of nickel (Ni) in the as-prepared nanocatalyst (in 10 mg of the nanocatalyst, 1.232 mg (or 0.020990435 mmol) of Ni has existed).

Scheme 6 Solvent-free one-pot *pseudo*-three-component synthesis of 9-aryl-3,3,6,6-tetramethyl-3,4,5,6,7,9-hexahydro-1*H*-xanthene-1,8(2*H*)-diones catalyzed by the as-prepared Fe_3O_4/*f*-MWCNT-CS-Glu/Ni^{II} nanocomposite.

2.4. Comparative study

To show the high value and efficiency of the presented Fe_3O_4/*f*-MWCNT-CS-Glu/Ni^{II} nanocomposite as a gigantic nanocatalytic system in the above-mentioned heterocyclic frameworks one-pot preparation, we compared it with some previously reported protocols on the synthesis of **3a**, **5a**, **7a**, and **9a**. As shown in Table 5, the new synthetic protocols which presented in this paper are better than others in terms of the catalyst loading, reaction time, favorable yield, use of green reaction mediums (water or solvent-free), and so on.

3. Experimental

3.1. Reagents, samples, and apparatus

All starting materials, reagents, and solvents were commercially available (purchased from Merck, Sigma-Aldrich, and Fluka companies) and used directly without further purification.

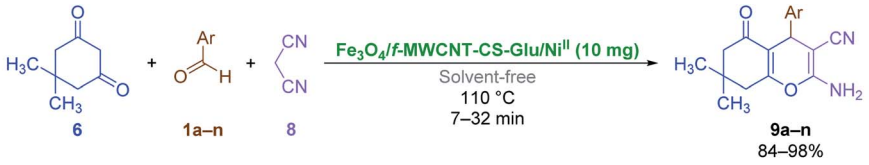

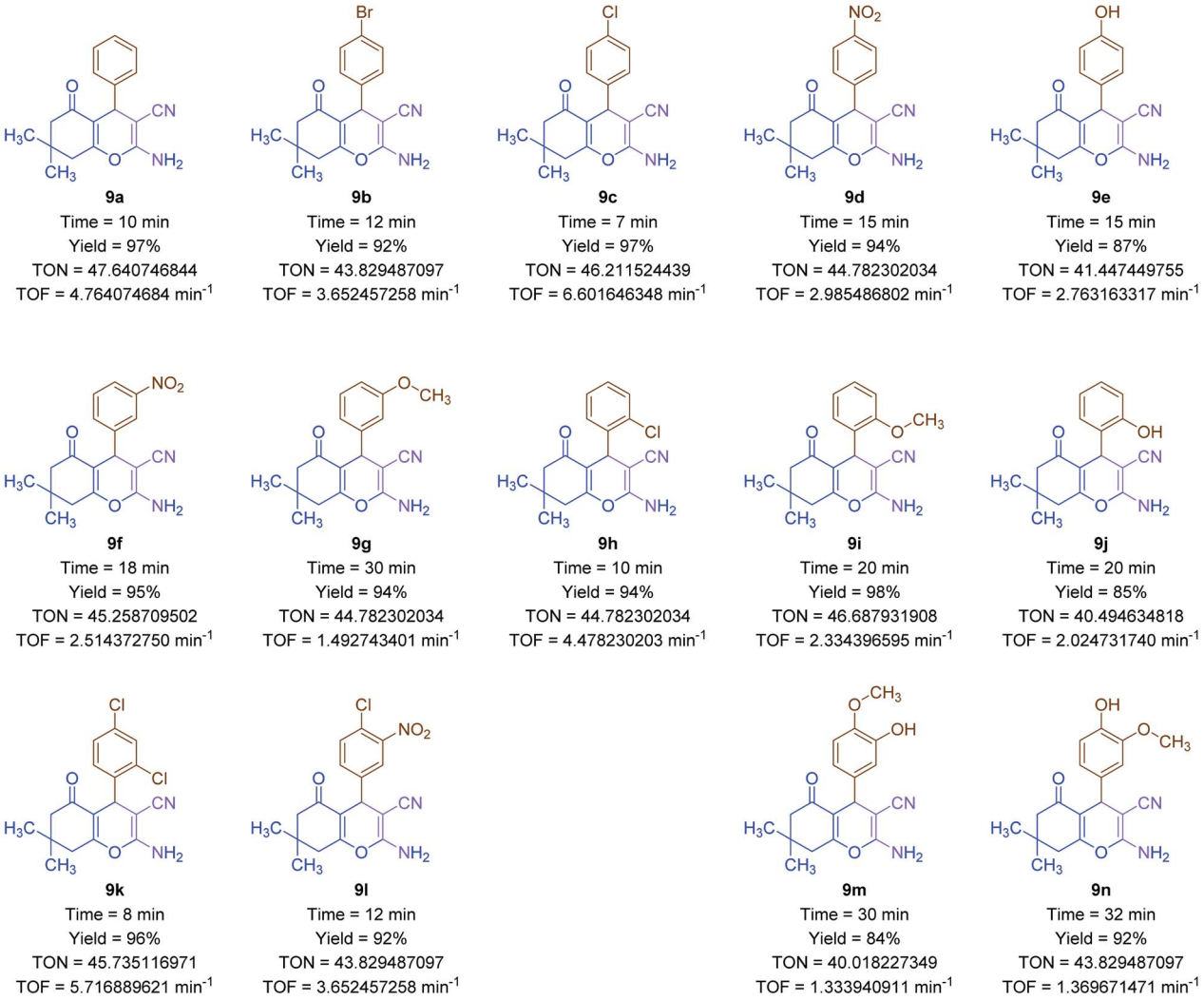

TON (Turnover number) = [(mol of product formed) / (mol of catalyst used)]
TOF (Turnover frequency) = [(mol of product formed) / (mol of catalyst used) × (time)]

Note:

The TONs and TOFs values were calculated based on the existed amount of nickel (Ni) in the as-prepared nanocatalyst (in 10 mg of the nanocatalyst, 1.232 mg (or 0.020990435 mmol) of Ni has existed).

Scheme 7 Solvent-free one-pot three-component synthesis of 2-amino-4-aryl-7,7-dimethyl-5-oxo-5,6,7,8-tetrahydro-4*H*-chromene-3-carbonitriles catalyzed by the as-prepared Fe_3O_4/*f*-MWCNT-CS-Glu/Ni^{II} nanocomposite.

SOLTEC SONICA 2400 MH S3 (300 W) instrument was used for ultrasonic irradiation. FT-IR spectra were recorded on Thermo Nicolet Nexus 670 spectrometer, and ^{1}H NMR spectra were obtained by Bruker Avance 300 MHz and 400 MHz spectrometer. The crystalline structures of the prepared nanocomposites were analyzed by powder X-ray diffraction (PXRD) on a Philips PANalytical X'PertPro diffractometer (Netherlands) in 40 kV and 30 mA with a monochromatized Cu Kα radiation ($\lambda = 1.5418$ Å). The SEM images, EDX diagram, and elemental mapping obtained from FESEM-TESCAN MIRA3 electronic microscope. The TEM images were obtained from Zeiss EM10C-100 kV transmission electron microscope. The elemental analysis was carried out by inductively coupled plasma-optical emission spectrometry (Optima 7300DV ICP-OES). The magnetic properties of the prepared samples were measured using a vibrating sample magnetometer (Meghnatis Daghigh, Iran) under magnetic fields up to 20 kOe.

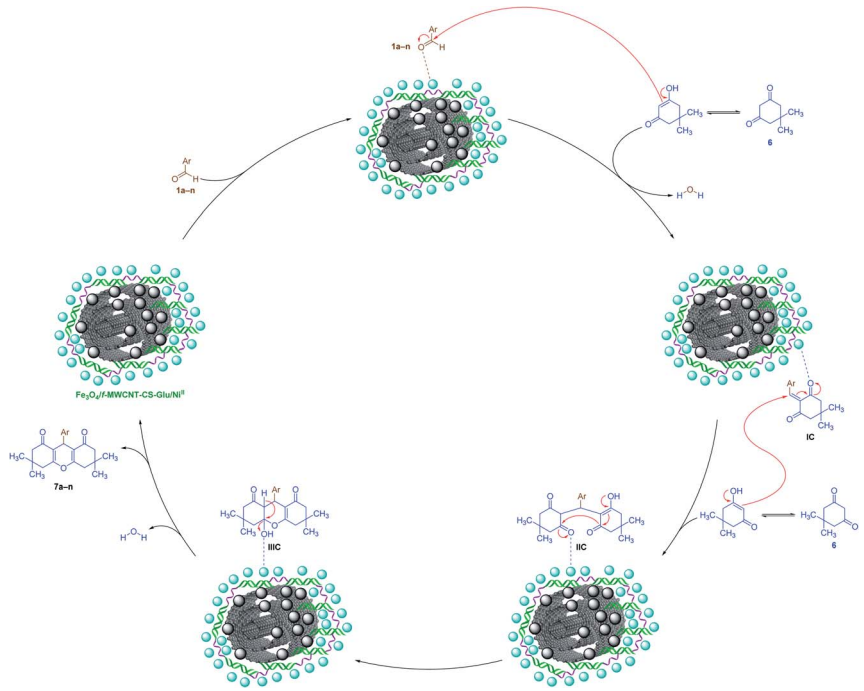

Scheme 8 Plausible mechanism for the solvent-free one-pot *pseudo*-three-component synthesis of 9-aryl-3,3,6,6-tetramethyl-3,4,5,6,7,9-hexahydro-1*H*-xanthene-1,8(2*H*)-diones catalyzed by the as-prepared Fe_3O_4/*f*-MWCNT-CS Glu/Ni^{II} nanocomposite.

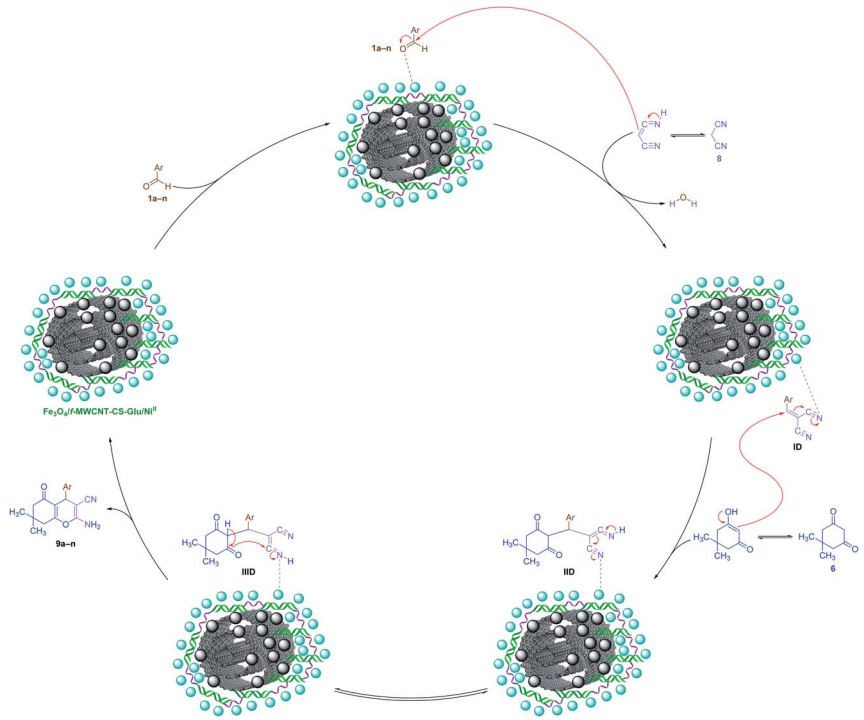

Scheme 9 Plausible mechanism for the solvent-free one-pot three-component synthesis of 2-amino-4-aryl-7,7-dimethyl-5-oxo-5,6,7,8-tetrahydro-4*H*-chromene-3-carbonitriles catalyzed by the as-prepared Fe_3O_4/*f*-MWCNT-CS-Glu/Ni^{II} nanocomposite.

3.2. One-pot preparation of the Fe_3O_4/*f*-MWCNT-CS-Glu nanocomposite

Firstly, in a three-necked round-bottom flask (250 mL), MWCNT-CO_2H (0.48 g) was dispersed in deionized water (100 mL) by ultrasonic irradiation for thirty minutes. Then, $Fe_3O_4 \cdot 6H_2O$ (0.6 g) and $FeCl_2 \cdot 4H_2O$ (0.45 g) were added into the mentioned pot and sonicated for another thirty minutes. After that, the 40 mL ammonia solution was added portion wisely into the reaction

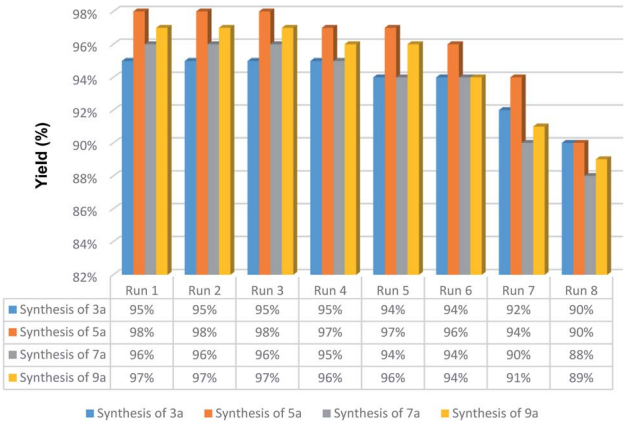

	Run 1	Run 2	Run 3	Run 4	Run 5	Run 6	Run 7	Run 8
Synthesis of 3a	95%	95%	95%	95%	94%	94%	92%	90%
Synthesis of 5a	98%	98%	98%	97%	97%	96%	94%	90%
Synthesis of 7a	96%	96%	96%	95%	94%	94%	90%	88%
Synthesis of 9a	97%	97%	97%	96%	96%	94%	91%	89%

Fig. 10 Recoverability and reusability experiments of the Fe_3O_4/*f*-MWCNT-CS-Glu/Ni^{II} nanocomposite.

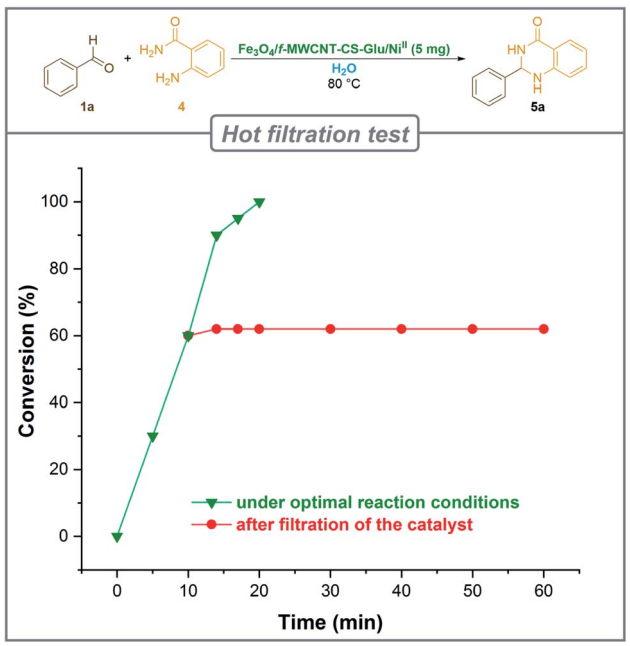

Fig. 11 Hot filtration test for the heterogeneity investigation of the Fe_3O_4/*f*-MWCNT-CS-Glu/Ni^{II} nanocomposite catalytic system.

environment at 60 °C under a nitrogen atmosphere and stirred for two hours. In the next step, the dissolved chitosan (0.18 g) in two percent acetic acid solution was added into the mentioned three-necked round-bottom flask and stirred for two hours at 60 °C under the nitrogen atmosphere. Finally, L-glutamic acid (0.2 g) was added to the reaction mixture and stirred for twenty hours under the same temperature and atmospheric conditions. The prepared Fe_3O_4/*f*-MWCNT-CS-Glu nanocomposite collected from the reaction pot, washed with deionized water and ethanol, and then dried at 50 °C.

3.3. Preparation of the Fe_3O_4/*f*-MWCNT-CS-Glu/Ni^{II} nanocomposite

In a round-bottom flask (100 mL), the prepared Fe_3O_4/*f*-MWCNT-CS-Glu (0.5 g) was dispersed in a 1 : 2 mixture of

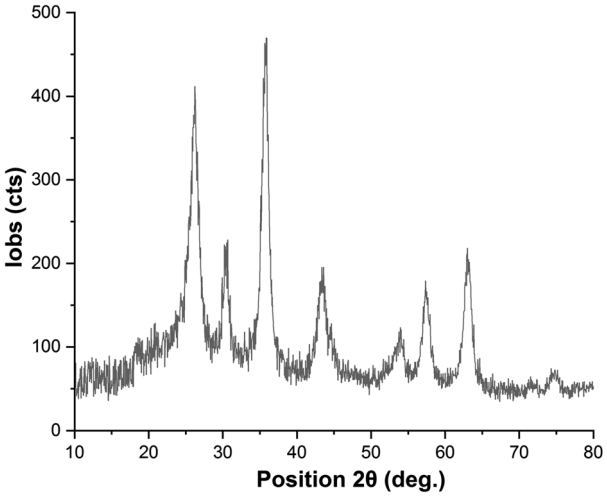

Fig. 12 PXRD diagram of the recycled Fe_3O_4/*f*-MWCNT-CS-Glu/Ni^{II} nanocomposite.

water and ethanol (70 mL) by ultrasonic irradiation for ten minutes. Next, nickel^{II} nitrate hexahydrate ($Ni(NO_3)_2 \cdot 6H_2O$) (0.25 g) was added into the mentioned reaction pot and sonicated for another forty-five minutes, and then stirred for twenty-four hours at 60 °C under air atmosphere. The as-prepared Fe_3O_4/*f*-MWCNT-CS-Glu/Ni^{II} nanocomposite collected from the reaction environment, washed with deionized water and ethanol, and then dried at 50 °C.

3.4. General procedure for the one-pot *pseudo*-three-component synthesis of bis-coumarins (3a–n) catalyzed by the as-prepared Fe_3O_4/*f*-MWCNT-CS-Glu/Ni^{II} nanocomposite

As a representative example, in a round-bottom flask (10 mL), which equipped with a magnetic stirrer, a mixture of benzaldehyde (1 mmol), 4-hydroxycoumarin (2 mmol), and the as-prepared Fe_3O_4/*f*-MWCNT-CS-Glu/Ni^{II} (5 mg) in the water solvent (3 mL) was prepared and stirred under reflux conditions for an appropriate time (10 minutes). As soon as the mentioned one-pot reaction was completed, the Fe_3O_4/*f*-MWCNT-CS-Glu/Ni^{II} nanocatalyst was separated from the reaction pot using an external magnet. Then, after cooling to room temperature, the resulting mixture was extracted with ethanol (2 × 5 mL), followed by drying over anhydrous sodium sulfate (Na_2SO_4). The solvent evaporation under reduced pressure affords the crude 3,3′-(phenylmethylene)bis(4-hydroxy-2*H*-chromen-2-one) (**3a**) product, which was subsequently purified by recrystallization from hot ethanol.

3.5. General procedure for the one-pot two-component synthesis of 2-aryl(or heteroaryl)-2,3-dihydroquinazolin-4(1*H*)-ones (5a–r) catalyzed by the as-prepared Fe_3O_4/*f*-MWCNT-CS-Glu/Ni^{II} nanocomposite

As a representative example, in a round-bottom flask (10 mL), which equipped with a magnetic stirrer, a mixture of benzaldehyde (1 mmol), anthranilamide (1 mmol), and the as-prepared Fe_3O_4/*f*-MWCNT-CS-Glu/Ni^{II} (5 mg) in the water

Table 5 Comparison of the catalytic activity of the as-prepared Fe_3O_4/*f*-MWCNT-CS-Glu/Ni^{II} nanocomposite with literature samples reported for the synthesis of **3a**, **5a**, **7a**, and **9a**

Entry	TM	Catalyst	Solvent	Reaction conditions	Time (min)	Yield (%)	Ref
1	**3a**	Fe_3O_4/*f*-MWCNT-CS-Glu/Ni^{II} (5 mg)	H_2O	Reflux	10	95	[a]
2	**3a**	HAP/Fe_3O_4 (5 mg)	Solvent-free	90 °C	60	95	32
3	**3a**	BFA (10 wt%)	H_2O	Room temperature	15	92	33
4	**3a**	Ni^0-Mont (20 mg)	Solvent-free	MW (850 W)	5	95	34
5	**3a**	Carbon-SO_3H (30 mg)	H_2O : CH_3CH_2OH (1 : 1)	80 °C	10	97	35
6	**3a**	P_4VPy-CuO (20 mg)	H_2O	Reflux	20	90	36
7	**3a**	RHA-SO_3H (40 mg)	H_2O	80 °C	15	90	37
8	**3a**	SO_3H@Fe_3O_4 (15 mg)	Solvent-free	80 °C	10	92	38
9	**3a**	SDS (20 mol%)	H_2O	60 °C	120	85	39
10	**3a**	$Fe(SD)_3$ (20 mol%)	H_2O	100 °C	10	79	40
11	**3a**	Fe_3O_4@SiO_2@Im-bisethylFc [HC_2O_4] (4 mg)	CH_3CH_2OH	Reflux	60	96	41
12	**3a**	Vitamin B_1 (1 mol%)	Solvent-free	Room temperature	60	92	42
13	**3a**	$(N_2H_5)_2SiF_6$ (0.2 mol%)	CH_3CH_2OH	Reflux	3	95	43
14	**5a**	Fe_3O_4/*f*-MWCNT-CS-Glu/Ni^{II} (5 mg)	H_2O	80 °C	20	98	[a]
15	**5a**	UiO-66-MW (1.2 mg)	CH_3CO_2H	60 °C	240	85	44
16	**5a**	VO-vanillin-MCM-41 (20 mg)	H_2O	90 °C	130	96	45
17	**5a**	$TiCl_3$/NFC (40 mg)	CH_3CH_2OH	Reflux	20	85	46
18	**5a**	Ompg-C_3N_4/SO_3H (20 mg)	CH_3CH_2OH	Reflux	3	98	47
19	**5a**	Zr-MOF/rGO (20 mg)	CH_3CH_2OH	55 °C	30	95	48
20	**5a**	SBA-15@*n*-Pr-THAM-ZrO (7 mg)	CH_3CH_2OH	Reflux	80	93	49
21	**5a**	$CoFe_2O_4$@Pr^{III} (50 mg)	CH_3CH_2OH	Reflux	60	97	50
22	**5a**	Ascorbic acid (10 mol%)	H_2O	90 °C	60	92	51
23	**5a**	Fe_3O_4@NCs-PA (40 mg)	H_2O : CH_3CH_2OH (1 : 1)	Reflux	90	83	52
24	**5a**	$CoFe_2O_4$@SiO_2-CPTES-guanidine-Cu^{II} (8 mg)	H_2O	80 °C	20	96	53
25	**5a**	$Cu(NO_3)_2$/Fe_3O_4-EDTA (10 mg)	H_2O	Reflux	30	98	54
26	**7a**	Fe_3O_4/*f*-MWCNT-CS-Glu/Ni^{II} (10 mg)	Solvent-free	110 °C	40	96	[a]
27	**7a**	Ag@Sep-N-CH (30 mg)	H_2O : CH_3CH_2OH (1 : 2)	50 °C	180	95	55
28	**7a**	Ag@CDNS-N/PMelamine (30 mg)	H_2O : CH_3CH_2OH (1 : 2)	50 °C	180	92	56
29	**7a**	SA@Sawdust (50 mg)	CH_3CH_2OH	Reflux	50	92	57
30	**7a**	[SO_3H-pyrazine-SO_3H]Cl_2 (0.25 mmol)	Solvent-free	110 °C	35	93	58
31	**7a**	[TMXH]$FeCl_4$ (0.25 mmol)	Solvent-free	110 °C	10	92	59
32	**7a**	UiO_2-66-NH_2-ILP F_6^--guanidine (30 mg)	CH_3CH_2OH	25 °C	45	95	60
33	**7a**	Fe_3O_4@THAM-piperazine (10 mg)	H_2O : CH_3CH_2OH (1 : 1)	100 °C	15	88	61
34	**7a**	NiFeTi CLDH6 (20 mg)	CH_3CH_2OH	80 °C	60	96	62
35	**7a**	Fe-X (25 mg)	Solvent-free	90 °C	15	95	63
36	**7a**	Fe_3O_4@NFC@NNS-Mn^{II} (10 mg)	CH_3CH_2OH	45 °C	10	98	64
37	**7a**	Cu^{II}-FUR-APTES/GO (20 mg)	H_2O : CH_3CH_2OH (1 : 1)	50 °C	30	95	65
38	**9a**	Fe_3O_4/*f*-MWCNT-CS-Glu/Ni^{II} (10 mg)	Solvent-free	110 °C	10	97	[a]
39	**9a**	Fe_3O_4@MCM-41@Zr (30 mg)	H_2O : CH_3CH_2OH (3 : 7)	75 °C	40	74	66
40	**9a**	Zn_2SnO_4–SnO_2 (25 mg)	CH_3CH_2OH	US (80 °C)	120	80	67
41	**9a**	AMBA-Fe_3O_4 (50 mg)	CH_3CH_2OH	60 °C	21	92	68

Table 5 (*Contd.*)

Entry	TM	Catalyst	Solvent	Reaction conditions	Time (min)	Yield (%)	Ref
42	**9a**	HMS/Pr-Rh-Zr (50 mg)	PEG	80 °C	30	87	69
43	**9a**	NH_2@SiO_2@Fe_3O_4 (10 mg)	Solvent-free	Grinding	4	94	70
44	**9a**	$BaFe_{12}O_{19}$@IM (12 mg)	CH_3CH_2OH	Reflux	20	88	71
45	**9a**	MNPs-$PhSO_3H$ (10 mg)	H_2O : CH_3CH_2OH (1 : 1)	100 °C	10	91	72
46	**9a**	Bis-Su (10 mg)	H_2O : CH_3CH_2OH (1 : 1)	80 °C	35	84	73
47	**9a**	Ni@Fe-doped CeO_2/Chitosan (10 wt%)	CH_3CH_2OH	60 °C	10	90	74
48	**9a**	Fe_3O_4@SiO_2-guanidine-PAA (50 mg)	H_2O	70 °C	35	96	75
49	**9a**	Fe_3O_4@GOQD-*O*-(propane-1-sulfonic acid) (50 mg)	H_2O	Room temperature	35	93	76

[a] Present work. TM = Target molecule. MW = Microwave. US = Ultrasonic.

solvent (3 mL) was prepared and stirred at 80 °C for twenty minutes. As soon as the mentioned one-pot reaction was completed, the Fe_3O_4/*f*-MWCNT-CS-Glu/Ni^{II} nanocatalyst was separated from the reaction pot using an external magnet. Then, after cooling to room temperature, the resulting mixture was extracted with ethanol (2 × 5 mL), followed by drying over Na_2SO_4. The solvent evaporation under reduced pressure affords the crude 2-phenyl-2,3-dihydroquinazolin-4(1*H*)-one (**5a**) product, which was subsequently purified by recrystallization from hot ethanol.

3.6. General procedure for the one-pot *pseudo*-three-component synthesis of 9-aryl-3,3,6,6-tetramethyl-3,4,5,6,7,9-hexahydro-1*H*-xanthene-1,8(2*H*)-diones (7a–n) catalyzed by the as-prepared Fe_3O_4/*f*-MWCNT-CS-Glu/Ni^{II} nanocomposite

As a representative example, in a simple experimental tube, which equipped with a magnetic stirrer, a mixture of benzaldehyde (1 mmol), 5,5-dimethyl-1,3-cyclohexanedione (dimedone) (2 mmol), and the as-prepared Fe_3O_4/*f*-MWCNT-CS-Glu/Ni^{II} (10 mg) was prepared and heated at 110 °C under solvent-free conditions for forty minutes. After completion of the mentioned one-pot *pseudo*-three-component reaction and cooling it to room temperature, ethanol (3 mL) was added and the reaction mixture was stirred for two minutes. Then, the Fe_3O_4/*f*-MWCNT-CS-Glu/Ni^{II} nanocatalyst was magnetically separated from the reaction environment. Next, the resulting solution was dried over Na_2SO_4. The solvent evaporation under reduced pressure affords the pure 9-phenyl-3,3,6,6-tetramethyl-3,4,5,6,7,9-hexahydro-1*H*-xanthene-1,8(2*H*)-dione (**7a**) product.

3.7. General procedure for the one-pot three-component synthesis of 2-amino-4-aryl-7,7-dimethyl-5-oxo-5,6,7,8-tetrahydro-4*H*-chromene-3-carbonitriles (9a–n) catalyzed by the as-prepared Fe_3O_4/*f*-MWCNT-CS-Glu/Ni^{II} nanocomposite

As a representative example, in a simple experimental tube, which equipped with a magnetic stirrer, a mixture of benzaldehyde (1 mmol), malononitrile (1 mmol), 5,5-dimethyl-1,3-cyclohexanedione (dimedone) (1 mmol), and the as-prepared Fe_3O_4/*f*-MWCNT-CS-Glu/Ni^{II} (10 mg) was prepared and heated at 110 °C under solvent-free conditions for ten minutes. After completion of the mentioned one-pot three-component reaction and cooling it to room temperature, ethanol (3 mL) was added and the reaction mixture was stirred for two minutes. Then, the Fe_3O_4/*f*-MWCNT-CS-Glu/Ni^{II} nanocatalyst was magnetically separated from the reaction environment. Next, the resulting solution was dried over Na_2SO_4. The solvent evaporation under reduced pressure affords the pure 2-amino-4-phenyl-7,7-dimethyl-5-oxo-5,6,7,8-tetrahydro-4*H*-chromene-3-carbonitrile (**9a**) product.

4. Conclusions

In summary, a novel magnetic nickel^{II}-containing nanocatalyst denoted as Fe_3O_4/*f*-MWCNT-CS-Glu/Ni^{II} was successfully fabricated and characterized by various techniques, including FT-IR, PXRD, SEM, TEM, SEM-based EDX and elemental mapping,

ICP-OES, TGA/DTA, and VSM. Interestingly, the as-prepared Fe_3O_4/*f*-MWCNT-CS-Glu/Ni^{II} hybrid nanosystem was an excellent catalyst for the preparation of various type of heterocyclic compounds, including bis-coumarins (**3a–n**), 2-aryl(or hetero-aryl)-2,3-dihydroquinazolin-4(1*H*)-ones (**5a–r**), 9-aryl-3,3,6,6-tetramethyl-3,4,5,6,7,9-hexahydro-1*H*-xanthene-1,8(2*H*)-diones (**7a–n**), and 2-amino-4-aryl-7,7-dimethyl-5-oxo-5,6,7,8-tetrahydro-4*H*-chromene-3-carbonitriles (**9a–n**) in good-to-excellent yields and satisfactory TONs and TOFs through the convenient and green one-pot multi-component synthetic procedures. Notably, other catalytic applications of the mentioned Fe_3O_4/*f*-MWCNT-CS-Glu/Ni^{II} magnetic nanocomposite are currently under investigation in our lab and will be reported in due course.

Conflicts of interest

There are no conflicts to declare.

Acknowledgements

The author thanks Urmia University for support of this work.

References

1 (*a*) W. Wang, Q. Meng, Q. Li, J. Liu, M. Zhou, Z. Jin and K. Zhao, *Int. J. Mol. Sci.*, 2020, **21**, 487; (*b*) L. A. Frank, G. R. Onzi, A. S. Morawski, A. R. Pohlmann, S. S. Guterres and R. V. Contri, *React. Funct. Polym.*, 2020, **147**, 104459; (*c*) Z. Shariatinia, *Int. J. Biol. Macromol.*, 2018, **120**, 1406–1419; (*d*) B. Sharma, S. Sharma and P. Jain, *Int. J. Biol. Macromol.*, 2021, **169**, 414–427; (*e*) L. Tian, A. Singh and A. V. Singh, *Int. J. Biol. Macromol.*, 2020, **153**, 533–538; (*f*) M. Kurakula and N. R. Naveen, *Int. J. Biol. Macromol.*, 2020, **165**, 1924–1938; (*g*) S. Kumar, J. Dutta, P. K. Dutta and J. Koh, *Int. J. Biol. Macromol.*, 2020, **160**, 470–481; (*h*) A. B. da Silva, K. B. Rufato, A. C. de Oliveira, P. R. Souza, E. P. da Silva, E. C. Muniz, B. H. Vilsinski and A. F. Martins, *Int. J. Biol. Macromol.*, 2020, **161**, 977–998; (*i*) X. Wang, H. S. Almoallim, Q. Cui, S. A. Alharbi and H. Yang, *Int. J. Biol. Macromol.*, 2021, **171**, 198–207.

2 (*a*) D. Wu, L. Zhu, Y. Li, X. Zhang, S. Xu, G. Yang and T. Delair, *Carbohydr. Polym.*, 2020, **238**, 116126; (*b*) R. Shanmuganathan, T. N. J. I. Edison, F. LewisOscar, P. Kumar, S. Shanmugam and A. Pugazhendhi, *Int. J. Biol. Macromol.*, 2019, **130**, 727–736; (*c*) A. Ali and S. Ahmed, *Int. J. Biol. Macromol.*, 2018, **109**, 273–286; (*d*) S. Pramanik and V. Sali, *Int. J. Biol. Macromol.*, 2021, **169**, 103–121.

3 (*a*) N. Saranya, A. Moorthi, S. Saravanan, M. P. Devi and N. Selvamurugan, *Int. J. Biol. Macromol.*, 2011, **48**, 234–238; (*b*) D. Chuan, T. Jin, R. Fan, L. Zhou and G. Guo, *Adv. Colloid Interface Sci.*, 2019, **268**, 25–38.

4 (*a*) I. M. van der Lubben, J. C. Verhoef, G. Borchard and H. E. Junginger, *Eur. J. Pharm. Sci.*, 2001, **14**, 201–207; (*b*) R. C. Red, S. C. Naylor, C. W. Potter, J. Bond, I. Jabbal-Gill, A. Fisher, L. Illum and R. Jennings, *Vaccine*, 2005, **23**, 4367–4374; (*c*) L. Xing, Y.-T. Fan, T. J. Zhou, J.-H. Gong, L.-H. Cui, K.-H. Cho, Y.-J. Choi, H. Jiang and C.-S. Cho, *Molecules*, 2018, **23**, 229.

5 (*a*) M. Cicciù, L. Fiorillo and G. Cervino, *Mar. Drugs*, 2019, **17**, 417; (*b*) E. Fakhri, H. Eslami, P. Maroufi, F. Pakdel, S. Taghizadeh, K. Gunbarov, M. Yousefi, A. Tanomand, B. Yousefi, S. Mahmoudi and H. Samadi Kafil, *Int. J. Biol. Macromol.*, 2020, **162**, 956–974; (*c*) C. Zhang, D. Hui, C. Du, H. Sun, W. Peng, X. Pu, Z. Li, J. Sun and C. Zhou, *Int. J. Biol. Macromol.*, 2021, **167**, 1198–1210.

6 (*a*) A. Di Martino, M. Sittinger and M. V. Risbud, *Biomaterials*, 2005, **26**, 5983–5990; (*b*) J.-K. F. Suh and H. W. T. Matthew, *Biomaterials*, 2000, **21**, 2589–2598; (*c*) J. Venkatesan and S.-K. Kim, *Mar. Drugs*, 2010, **8**, 2252–2266; (*d*) S. Ranganthan, K. Balagangadharan and N. Selvamurugan, *Int. J. Biol. Macromol.*, 2019, **133**, 354–364; (*e*) S. Khan, M. Garg, S. Chockalingam, P. Gopinath and P. P. Kundu, *Int. J. Biol. Macromol.*, 2020, **143**, 285–296; (*f*) M. Tamimi, S. Rajabi and M. Pezeshki-Modaress, *Int. J. Biol. Macromol.*, 2020, **164**, 389–402.

7 (*a*) A. Moeini, P. Pedram, P. Makvandi, M. Malinconico and G. Gomez d'Ayala, *Carbohydr. Polym.*, 2020, **233**, 115839; (*b*) S. S. Biranje, P. V. Madiwale, K. C. Patankar, R. Chhabra, P. Dandekar-Jain and R. V. Adivarekar, *Int. J. Biol. Macromol.*, 2019, **121**, 936–946; (*c*) M. Ishihara, K. Nakanishi, K. Ono, M. Sato, M. Kikuchi, Y. Saito, H. Yura, T. Matsui, H. Hattori, M. Uenoyama and A. Kurita, *Biomaterials*, 2002, **23**, 833–840; (*d*) P. S. Kaparekar, S. Pathmanapan and S. K. Anandasadagopan, *Int. J. Biol. Macromol.*, 2020, **165**, 930–947; (*e*) A. Mazloom-Jalili, Z. Shariatinia, I. Ashrafi Tamai, S.-R. Pakzad and J. Malakootikhah, *Int. J. Biol. Macromol.*, 2020, **153**, 421–432; (*f*) N. Sakthiguru and M. A. Sithique, *Int. J. Biol. Macromol.*, 2020, **152**, 873–883.

8 (*a*) P. M. Pakdel and S. J. Peighambardoust, *Carbohydr. Polym.*, 2018, **201**, 264–279; (*b*) J. Desbrières and E. Guibal, *Polym. Int.*, 2018, **67**, 7–14; (*c*) S. Sarode, P. Upadhyay, M. A. Khosa, T. Mak, A. Shakir, S. Song and A. Ullah, *Int. J. Biol. Macromol.*, 2019, **121**, 1086–1100.

9 (*a*) R. L. Kashyap, X. Xiang and P. Heiden, *Int. J. Biol. Macromol.*, 2015, **77**, 36–51; (*b*) B. Qu and Y. Luo, *Int. J. Biol. Macromol.*, 2020, **152**, 437–448; (*c*) K. B. M. Ahmed, M. M. A. Khan, H. Siddiqui and A. Jahan, *Carbohydr. Polym.*, 2020, **227**, 115331; (*d*) R. C. Choudhary, R. V. Kumaraswamy, S. Kumari, S. S. Sharma, A. Pal, R. Raliya, P. Biswas and V. Saharan, *Int. J. Biol. Macromol.*, 2019, **127**, 126–135; (*e*) G. L. Vanti, S. Masaphy, M. Kurjogi, S. Chakrasali and V. B. Nargund, *Int. J. Biol. Macromol.*, 2020, **156**, 1387–1395.

10 (*a*) K. Rambabu, G. Bharath, F. Banat, P. L. Show and H. Hernández Cocoletzi, *Int. J. Biol. Macromol.*, 2019, **126**, 1234–1243; (*b*) S. Kumar, A. Makherjee and J. Dutta, *Trends Food Sci. Technol.*, 2020, **97**, 196–209; (*c*) H. Wang, J. Qian and F. Ding, *J. Agric. Food Chem.*, 2018, **66**, 395–413; (*d*) L. O. Xavier, W. G. Sganzerla, G. B. Rosa, C. G. Da Rosa, L. Agostinetto, A. P. De Lima Veeck, L. C. Bretanha, G. A. Micke, M. D. Costa, F. C. Bertodi, P. L. M. Barreto and M. R. Nunes, *Int. J. Biol. Macromol.*, 2021, **169**, 183–193.

11 (*a*) H. Mousavi, *Int. J. Biol. Macromol.*, 2021, **186**, 1003–1166; (*b*) Á. Molnár, *Coord. Chem. Rev.*, 2019, **388**, 126–171; (*c*) A. Dhakshinamoorthy, M. Jacob, N. S. Vignesh and P. Varalakshmi, *Int. J. Biol. Macromol.*, 2021, **167**, 807–833; (*d*) M. Dohendou, K. Pakzad, Z. Nezafat, M. Nasrollahzadeh and M. G. Dekamin, *Int. J. Biol. Macromol.*, 2021, **192**, 771–819.

12 F. Ghaffarian, M. A. Ghasemzadeh and S. S. Aghaei, *J. Mol. Struct.*, 2019, **1186**, 204–211.

13 L.-G. Ding, B.-J. Yao, F. Li, S.-C. Shi, N. Huang, H.-B. Yin, Q. Guan and Y.-B. Dong, *J. Mater. Chem. A*, 2019, **7**, 4689–4698.

14 (*a*) M. Maleki and R. Paydar, *RSC Adv.*, 2015, **5**, 33177–33184; (*b*) A. Maleki and R. Paydar, *React. Funct. Polym.*, 2016, **109**, 120–124; (*c*) S. Kumar, M. Y. Wani, J. Koh, J. M. Gil and A. J. F. N. Sobral, *J. Environ. Sci.*, 2018, **69**, 77–84; (*d*) M. Mahdavinasab, M. Hamzehlouian and Y. Sarrafi, *Int. J. Biol. Macromol.*, 2019, **138**, 764–772.

15 (*a*) J. Sun, J. Wang, W. Cheng, J. Zhang, X. Li, S. Zhang and Y. She, *Green Chem.*, 2012, **14**, 654–660; (*b*) C. Jing-Xian, J. Bi, D. Wei-Li, D. Sen-Lin, C. Liu-Ren, C. Zong-Jie, L. Sheng-Lian, L. Xu-Biao, T. Xin-Man and A. Chak-Tong, *Appl. Catal., A*, 2014, **484**, 26–32; (*c*) M. Taheri, M. Ghiaci and A. Shchukarev, *New J. Chem.*, 2018, **42**, 587–597; (*d*) M. U. Khan, S. Siddiqui and Z. N. Siddiqui, *ACS Omega*, 2019, **4**, 7586–7595; (*e*) A. Khalafi-Nezhad and S. Mohammadi, *RSC Adv.*, 2013, **3**, 4362–4371.

16 (*a*) M. Chtchigrovsky, A. Primo, P. Gonzalez, K. Molvinger, M. Robitzer, F. Quignard and F. Taran, *Angew. Chem., Int. Ed.*, 2009, **48**, 5916–5920; (*b*) Anuradha, S. Layek, B. Agrahari and D. D. Pathak, *ChemistrySelect*, 2017, **2**, 6865–6876; (*c*) H. Naeimi and S. Lahouti, *Appl. Organomet. Chem.*, 2017, **31**, e3732; (*d*) H. Naeimi and S. Lahouti, *Transition Met. Chem.*, 2018, **43**, 221–229; (*e*) J. Rakhtshah and F. Yaghoobi, *Int. J. Biol. Macromol.*, 2019, **139**, 904–916.

17 K. C. Basavaraju, S. Sharma, A. K. Singh, D. J. Im and D.-P. Kim, *ChemSusChem*, 2014, **7**, 1864–1869.

18 (*a*) S. Philippe and E. Castillejos, *ChemCatChem*, 2010, **2**, 41–47; (*b*) V. Campisciano, M. Gruttadauria and F. Giacalone, *ChemCatChem*, 2019, **11**, 90–133; (*c*) A. C. Ghogia, A. Nzihou, P. Serp, K. Soulantica and D. P. Minh, *Appl. Catal., A*, 2021, **609**, 117906; (*d*) S. Ansari, A. Khorshidi and S. Shariati, *RSC Adv.*, 2020, **10**, 3554–3565; (*e*) M. S. Ghasemzadeh and B. Akhlaghinia, *ChemistrySelect*, 2019, **4**, 1542–1555.

19 (*a*) S. Chatterjee, M. W. Lee and S. H. Woo, *Carbon*, 2009, **47**, 2933–2939; (*b*) S. Karbasi and Z. M. Alizadeh, *Bull. Mater. Sci.*, 2017, **40**, 1247–1253; (*c*) I. M. Garnica-Palafox, H. O. Estrella-Monroy, N. A. Vázquez-Torres, M. Áalvarez-Camacho, A. E. Castell-Rodríguez and F. M. Sánchez-Arévalo, *Carbohydr. Polym.*, 2020, **236**, 115971.

20 (*a*) V. Polshetiwar, R. Luque, A. Fihri, H. Zhu, M. Bouhara and J.-M. Basset, *Chem. Rev.*, 2011, **111**, 3036–3075; (*b*) S. Shylesh, V. Schünemann and W. R. Thiel, *Angew. Chem., Int. Ed.*, 2010, **49**, 3428–3459; (*c*) D. Wang and D. Astruc, *Chem. Rev.*, 2014, **114**, 6949–6985; (*d*) M. B. Gawande, R. Luque and R. Zboril, *ChemCatChem*, 2014, **6**, 3312–3313; (*e*) B. Karimi, F. Mansouri and H. M. Mirzaei, *ChemCatChem*, 2015, **7**, 1736–1789; (*f*) G. Mohammadi Ziarani, Z. Kheilkordi, F. Mohajer, A. Badiei and R. Luque, *RSC Adv.*, 2021, **11**, 17456–17477; (*g*) A. Pawar, S. Gajare, A. Patil, R. Kurane, G. Rashinkar and S. Patil, *Res. Chem. Intermed.*, 2021, **47**, 2801–2820; (*h*) M. Aghaei-Hashjin, A. Yahyazadeh and E. Abbaspour-Gilandeh, *RSC Adv.*, 2021, **11**, 23491–23505; (*i*) F. Mohammadsaleh, M. Dehdashti Jahromi, A. R. Hajipour, S. M. Hosseini and K. Niknam, *RSC Adv.*, 2021, **11**, 20812–20823; (*j*) N. Hosseini Mohtasham and M. Gholizadeh, *Res. Chem. Intermed.*, 2021, **47**, 2507–2525; (*k*) A. Naikwade, M. Jagadale, D. Kale and G. Rashinkar, *Aust. J. Chem.*, 2020, **73**, 1088–1097; (*l*) M. Mohammadi and A. Ghorbani-Choghamarani, *RSC Adv.*, 2022, **12**, 2770–2787.

21 (*a*) B. Eftekhari-Sis, M. Zirak and A. Akbari, *Chem. Rev.*, 2013, **113**, 2958–3043; (*b*) B. Eftekhari-Sis and M. Zirak, *Chem. Rev.*, 2015, **115**, 151–264.

22 (*a*) A. Dömling, W. Wang and K. Wang, *Chem. Rev.*, 2012, **112**, 3083–3135; (*b*) S. Abu-Melha, Z. A. Muhammad, A. S. Abouzid, M. M. Edrees, A. S. Abo Dena, S. Nabil and S. M. Gomha, *J. Mol. Struct.*, 2021, **1234**, 130180; (*c*) H. G. O. Alvim, E. N. da Silva Júnior and B. A. D. Neto, *RSC Adv.*, 2014, **4**, 54282–54299; (*d*) S. Kamalifar and H. Kiyani, *Res. Chem. Intermed.*, 2019, **45**, 5975–5987; (*e*) L. Wu, S. Yan, W. Wang and Y. Li, *Res. Chem. Intermed.*, 2020, **46**, 4311–4322; (*f*) A. Patil, S. Shinde, G. Rashinkar and R. Salunkhe, *Res. Chem. Intermed.*, 2020, **46**, 63–73; (*g*) S. Zhi, X. Ma and W. Zhang, *Org. Biomol. Chem.*, 2019, **17**, 7632–7650; (*h*) N. Nikooei, M. G. Dekamin and E. Valiey, *Res. Chem. Intermed.*, 2020, **46**, 3891–3909; (*i*) M. Rimaz and H. Mousavi, *Turk. J. Chem.*, 2013, **37**, 252–261; (*j*) M. Rimaz, H. Mousavi, L. Ozzar and B. Khalili, *Res. Chem. Intermed.*, 2019, **45**, 2673–2694; (*k*) M. Rimaz, H. Mousavi, B. Khalili and L. Sarvari, *J. Iran. Chem. Soc.*, 2019, **16**, 1687–1701; (*l*) M. Rimaz, B. Khalili, G. Khatyal, H. Mousavi and F. Aali, *Aust. J. Chem.*, 2017, **70**, 1274–1284; (*m*) M. Rimaz, H. Mousavi, M. Behnam, L. Sarvari and B. Khalili, *Curr. Chem. Lett.*, 2017, **6**, 55–68; (*n*) M. Rimaz, H. Mousavi, L. Nikpey and B. Khalili, *Res. Chem. Intermed.*, 2017, **43**, 3925–3937; (*o*) M. Rimaz, H. Mousavi, P. Keshavarz and B. Khalili, *Curr. Chem. Lett.*, 2015, **4**, 159–168; (*p*) P. Mane, B. Shinde, P. Mundada, B. Karale and A. Burungale, *Res. Chem. Intermed.*, 2021, **47**, 1743–1758; (*q*) I. Yellapurkar, S. Bhabal, M. M. V. Ramana, K. Jangam, V. Salve, S. Patange and P. More, *Res. Chem. Intermed.*, 2021, **47**, 2669–2687; (*r*) R. L. Mohlala, E. M. Coyanis, M. A. Fernandes and M. L. Bode, *RSC Adv.*, 2021, **11**, 24466–24473; (*s*) F. Haji Norouzi, N. Foroughifar, A. Khajeh-Amiri and H. Pasdar, *RSC Adv.*, 2021, **11**, 29948–29959; (*t*) B. M. Bizzarri, A. Fanelli, L. Botta, M. De Angelis, A. T. Palamara, L. Nencioni and R. Saladino, *RSC Adv.*, 2021, **11**, 30020–30029; (*u*) Z. Ghanbari and H. Naeimi, *RSC Adv.*, 2021, **11**, 31377–31384; (*v*) P. Ghamari Kargar, G. Bagherzade and H. Eshghi, *RSC Adv.*, 2021, **11**, 4339–4355; (*w*) P. Ghamari Kargar and G. Bagherzade, *RSC Adv.*, 2021, **11**, 23192–23206; (*x*) P. Ghamari Kargar, M. Noorian,

E. Chamani, G. Bagherzade and Z. Kiani, *RSC Adv.*, 2021, **11**, 17413–17430; (*y*) S. D. Dhengale, C. V. Rode, G. B. Kolekar and P. V. Anbhule, *RSC Adv.*, 2022, **12**, 2083–2093; (*z*) A. Ghasemi-Ghahsareh, J. Safaei-Ghomi and H. S. Oboudatian, *RSC Adv.*, 2022, **12**, 1319–1330; (*aa*) S. K. Dangolian, E. Niknam, O. Shahraki and A. Khalafi-Nezhad, *J. Mol. Struct.*, 2021, **1245**, 131061; (*ab*) F. Kamali and F. Shirini, *J. Mol. Struct.*, 2021, **1227**, 129654; (*ac*) S. Saeedi and A. Rahmati, *RSC Adv.*, 2022, **12**, 11740–11749; (*ad*) B. Borah, J. Bora, P. Ramesh and L. R. Chowhan, *RSC Adv.*, 2022, **12**, 12843–12857; (*ae*) M. Rimaz, H. Mousavi, B. Khalili and F. Aali, *J. Chin. Chem. Soc.*, 2018, **65**, 1389–1397.

23 (*a*) H. C. Erythropel, J. B. Zimmerman, T. M. de Winter, L. Petitjean, F. Melnikov, C. H. Lam, A. W. Lounsbury, K. E. Mellor, N. Z. Janković, Q. Tu, L. N. Pincus, M. M. Falinski, W. Shi, P. Coish, D. L. Plata and P. A. Anastas, *Green Chem.*, 2018, **20**, 1929–1961; (*b*) M. Pérez-Venegas and E. Juaristi, *ACS Sustainable Chem. Eng.*, 2020, **8**, 8881–8893; (*c*) M. C. Bryan, B. Dillon, L. G. Hamann, G. J. Hughes, M. E. Kopach, E. A. Peterson, M. Pourashraf, I. Raheem, P. Richardson, D. Richter and H. F. Sheddon, *J. Med. Chem.*, 2013, **56**, 6007–6021; (*d*) G. Náray-Szabó and L. T. Mika, *Green Chem.*, 2018, **20**, 2171–2191; (*e*) P. T. Anastas and J. B. Zimmerman, *Green Chem.*, 2019, **21**, 6545–6566; (*f*) M. Rimaz, Z. Jalalian, H. Mousavi and R. H. Prager, *Tetrahedron Lett.*, 2016, **57**, 105–109; (*g*) M. Rimaz, H. Mousavi, M. Behnam and B. Khalili, *Curr. Chem. Lett.*, 2016, **5**, 145–154.

24 (*a*) R. N. Butler and A. C. Coyne, *Chem. Rev.*, 2010, **110**, 6302–6337; (*b*) A. Chanda and V. V. Fokin, *Chem. Rev.*, 2009, **109**, 725–748; (*c*) M. Rimaz, J. Khalafy, H. Mousavi, S. Bohlooli and B. Khalili, *J. Heterocycl. Chem.*, 2017, **54**, 3174–3186; (*d*) M. Rimaz, J. Khalafy and H. Mousavi, *Res. Chem. Intermed.*, 2016, **42**, 8185–8200; (*e*) M. H. Sayahi, S. Bahadorikhalili, S. J. Saghanezhad, M. A. Miller and M. Mahdavi, *Res. Chem. Intermed.*, 2020, **46**, 491–507; (*f*) H. Mousavi, *J. Mol. Struct.*, 2021, **1251**, 131742.

25 (*a*) M. A. P. Martins, C. P. Frizzo, D. N. Moreira, L. Buriol and P. Machado, *Chem. Rev.*, 2009, **109**, 4140–4182; (*b*) M. S. Singh and S. Chowdhury, *RSC Adv.*, 2012, **2**, 4547–4592; (*c*) M. Tavakolian, S. Vahdati-Khajeh and S. Asgari, *ChemCatChem*, 2019, **11**, 2943–2977.

26 (*a*) H. Mousavi, B. Zeynizadeh, R. Younesi and M. Esmati, *Aust. J. Chem.*, 2018, **71**, 595–660; (*b*) B. Zeynizadeh, R. Younesi and H. Mousavi, *Res. Chem. Intermed.*, 2018, **44**, 7331–7352; (*c*) B. Zeynizadeh, F. Mohammad Aminzadeh and H. Mousavi, *Res. Chem. Intermed.*, 2019, **45**, 3329–3357; (*d*) B. Zeynizadeh, H. Mousavi and S. Zarrin, *J. Chin. Chem. Soc.*, 2019, **66**, 928–933; (*e*) B. Zeynizadeh, F. Mohammad Aminzadeh and H. Mousavi, *Green Process. Synth.*, 2019, **8**, 742–755; (*f*) B. Zeynizadeh, F. Sepehraddin and H. Mousavi, *Ind. Eng. Chem. Res.*, 2019, **58**, 16379–16388; (*g*) R. Bakhshi, B. Zeinizadeh and H. Mousavi, *J. Chin. Chem. Soc.*, 2020, **67**, 623–637; (*h*) B. Zeynizadeh, H. Mousavi and F. Sepehraddin, *Res. Chem. Intermed.*, 2020, **46**, 3361–3382; (*i*) B. Zeynizadeh, F. Mohammad Aminzadeh and H. Mousavi, *Res. Chem. Intermed.*, 2021, **47**, 3289–3312; (*j*) B. Zeynizadeh, H. Mousavi and F. Mohammad Aminzadeh, *J. Mol. Struct.*, 2022, **1253**, 131926; (*k*) M. Hasanpour Galehban, B. Zeynizadeh and H. Mousavi, *RSC Adv.*, 2022, **12**, 11164–11189.

27 S. Nisar, A. S. Pandit, M. Nadeem, A. H. Pandit, M. M. A. Rizvi and S. Rattan, *Int. J. Biol. Macromol.*, 2021, **182**, 37–50.

28 (*a*) J. Singh, P. K. Dutta, J. Dutta, A. J. Hunt, D. J. Macquarrie and J. H. Clark, *Carbohydr. Polym.*, 2009, **76**, 188–195; (*b*) J. A. Sirviö, A. M. Kantola, S. Komulainen and S. Filonenko, *Biomacromolecules*, 2021, **22**, 2119–2128; (*c*) M. Esfandiari, A. K. Abbas, M. R. Vakili, H. Shahbazi-Alavi and J. Safaei-Ghomi, *Res. Chem. Intermed.*, 2021, **47**, 483–496.

29 J. M. Tan, S. Bullo, S. Fakurazi and M. Z. Hussein, *Sci. Rep.*, 2020, **10**, 16941.

30 (*a*) P. C. Rath, B. P. Singh, L. Bersa and S. Bhattacharjee, *J. Am. Chem. Soc.*, 2012, **95**, 2725–2731; (*b*) M. A. Gizawy, H. A. Shamsel-Din, I. M. Abdelmonem, M. I. A. Ibrahim, L. A. Mohamed and E. Metwally, *Int. J. Biol. Macromol.*, 2020, **163**, 79–86; (*c*) R. Afshari, S. E. Hooshmand, M. Atharnezhad and A. Shaabani, *Polyhedron*, 2020, **175**, 114238.

31 (*a*) G. Yang, C. Cheng, G.-B. Xu, L. Tang, K.-L. Chua and Y.-Y. Yang, *Bioorg. Med. Chem.*, 2020, **28**, 115606; (*b*) N. S. O'Brein and A. McCluskey, *Aust. J. Chem.*, 2020, **73**, 1176–1186; (*c*) G. Yashwantro, V. P. Jejukar, R. Kshatriya and S. Saha, *ACS Sustainable Chem. Eng.*, 2019, **7**, 13551–13558; (*d*) Z. Lin, J. Qian, P. Lu and Y. Wang, *J. Org. Chem.*, 2020, **85**, 11766–11777; (*e*) S. Balaji, G. Balamurugan, R. Ramesh and D. Semeril, *Organometallics*, 2021, **40**, 725–734.

32 B. Akhlaghinia, P. Sanati, A. Mohammadinezhad and Z. Zarei, *Res. Chem. Intermed.*, 2019, **45**, 3215–3235.

33 C. Patil, S. K. Shinde, U. P. Patil, A. T. Birajdar and S. S. Patil, *Res. Chem. Intermed.*, 2021, **47**, 1675–1691.

34 S. Rahmani and B. Zeynizadeh, *Res. Chem. Intermed.*, 2019, **45**, 1227–1248.

35 D. K. Agarwal, A. Sethiya, P. Teli, A. Manhas, J. Sani, N. Sahiba, P. C. Jha, S. Agarwal and P. K. Goyal, *J. Heterocycl. Chem.*, 2020, **57**, 3294–3309.

36 F. Shirini, A. Fallah-Shojaei, L. Samavi and M. A. Abedini, *RSC Adv.*, 2016, **6**, 48469–48478.

37 M. Seddighi, F. Shirini and M. Mamaghani, *RSC Adv.*, 2013, **3**, 24046–24053.

38 X. Wu and W.-X. Peng, *J. Chin. Chem. Soc.*, 2020, **67**, 2129–2148.

39 H. Mehrabi and H. Abusaidi, *J. Iran. Chem. Soc.*, 2010, **7**, 890–894.

40 N. O. Mahmoodi, Z. Jalalifard and G. Pirbasti Fathanbari, *J. Chin. Chem. Soc.*, 2020, **67**, 172–182.

41 R. Teimuri-Mofrad, S. Tahmasebi and E. Payami, *Appl. Organomet. Chem.*, 2019, **33**, e4773.

42 S. Mathavan, K. Kannan and R. B. R. D. Yamajala, *Org. Biomol. Chem.*, 2019, **17**, 9620–9626.

43 E. El hajri, Z. Benzekri, S. Sibous, A. Ouasri, S. Boukhris, A. Hassikou, A. Rhandour and A. Souizi, *J. Mol. Struct.*, 2021, **1230**, 129890.

44 L. H. T. Nguyen, T. T. T. Nguyen, Y. T. Dang, P. H. Tran and T. L. H. Doan, *Asian J. Org. Chem.*, 2019, **8**, 2276–2281.
45 M. Nikoorazm and M. Khanmoradi, *J. Chin. Chem. Soc.*, 2020, **67**, 1477–1489.
46 H. Heidari, K. Nikoofar and Y. Shahedi, *Iran. J. Catal.*, 2019, **9**, 71–77.
47 H. Ghafuri, N. Goodarzi, A. Rashidzadeh and M. A. Douzandegi Fard, *Res. Chem. Intermed.*, 2019, **45**, 5027–5043.
48 G. Kumar, N. K. Mogha and D. T. Masram, *ACS Appl. Nano Mater.*, 2021, **4**, 2682–2693.
49 A. Ghorbani-Choghamarani, H. Aghavandi and M. Mohammadi, *J. Porous Mater.*, 2021, **28**, 1167–1186.
50 T. Tamoradi, S. M. Mousavi and M. Mohammadi, *New J. Chem.*, 2020, **44**, 3012–3020.
51 G. C. Pariyar, B. Mitra, S. Mukherjee and P. Ghosh, *ChemistrySelect*, 2020, **5**, 104–108.
52 B. B. F. Mirjalili, Z. Zaghaghi and A. Monfared, *J. Chin. Chem. Soc.*, 2020, **67**, 197–201.
53 L. Heidari and L. Shiri, *Appl. Organomet. Chem.*, 2019, **33**, e4636.
54 L. Shiri, A. Ghorbani-Choghamarani and M. Kazemi, *Appl. Organomet. Chem.*, 2019, **33**, e4636.
55 F. Ghoreyshi Kahangi, M. Mehrdad, M. M. Heravi and S. Sadjadi, *Sci. Rep.*, 2020, **10**, 15285.
56 S. Sadjadi, F. Ghoreyshi Kahangi, M. Dorraj and M. M. Heravi, *Molecules*, 2020, **25**, 241.
57 S. Karhale, *Res. Chem. Intermed.*, 2020, **46**, 3085–3096.
58 S. E. Sadati Sorkhi, M. M. Hashemi and A. Ezabadi, *Res. Chem. Intermed.*, 2020, **46**, 2229–2246.
59 M. Salami and A. Ezabadi, *Res. Chem. Intermed.*, 2020, **46**, 4611–4626.
60 S. Askari, M. M. Khodaei and M. Jafarzadeh, *Res. Chem. Intermed.*, 2021, **47**, 2881–2899.
61 H. Foroughi Niya, N. Hazeri, M. Fatahpour and M. T. Maghsoodlou, *Res. Chem. Intermed.*, 2020, **46**, 3651–3666.
62 G. Rathee, S. Kohli, N. Singh, A. Awasthi and R. Chandra, *ACS Omega*, 2020, **5**, 15673–15680.
63 S. F. Hojati, M. Moosavifar and N. Moeinieghbali, *J. Chem. Sci.*, 2020, **132**, 38.
64 P. G. Kargar, G. Bagherzadeh and H. Eshghi, *RSC Adv.*, 2021, **11**, 4339–4355.
65 Subodh, N. K. Mogha, K. Chaudhary, G. Kumar and D. T. Masram, *ACS Omega*, 2018, **3**, 16377–16385.
66 R. Pourhasan-Kisomi, F. Shirini and M. Golshekan, *Appl. Organomet. Chem.*, 2018, **32**, e4371.
67 M. Ziyaadini, N. Nemat-Bakhsh, S. J. Roudbaraki and M. Ghashang, *Polycyclic Aromat. Compd.*, 2022, **42**, 460–474.
68 M. M. Khodaei, A. Alizadeh and M. Haghipour, *Res. Chem. Intermed.*, 2020, **46**, 1033–1045.
69 S. Abdolahi, M. Hajjami and F. Gholamian, *Res. Chem. Intermed.*, 2021, **47**, 1883–1904.
70 P. Singh, P. Yadav, A. Mishra and S. K. Awasthi, *ACS Omega*, 2020, **5**, 4223–4232.
71 S. Amirnejat, A. Nosrati, R. Peymanfar and S. Javanshir, *Res. Chem. Intermed.*, 2020, **46**, 3683–3701.
72 H. Foroughi Niya, N. Hazeri, M. Rezaie Kahkhaie and M. T. Maghsoodlou, *Res. Chem. Intermed.*, 2020, **46**, 1685–1704.
73 F. Hasaanzadeh, N. Daneshvar, F. Shirini and M. Mamaghani, *Res. Chem. Intermed.*, 2020, **46**, 4971–4984.
74 A. Mahajan and M. Gupta, *Appl. Organomet. Chem.*, 2021, **35**, e6161.
75 P. Mohammadi and H. Sheibani, *Mater. Chem. Phys.*, 2019, **228**, 140–146.
76 M. Khaleghi Abbasabadi, D. Azarifar and H. R. Esmaili Zand, *Appl. Organomet. Chem.*, 2020, **34**, e6004.